

SSTRED: A data- and metadata-processing pipeline for CHROMIS and CRISP

Mats G. Löfdahl¹, Tomas Hillberg¹, Jaime de la Cruz Rodríguez¹, Gregal Vissers¹, Oleksii Andriienko¹, Göran B. Scharmer¹, Stein V. H. Haugan², and Terje Fredvik²

¹ Institute for Solar Physics, Dept. of Astronomy, Stockholm University, Albanova University Center, 106 91 Stockholm, Sweden

² Institute of Theoretical Astrophysics, University of Oslo, Postboks 1029, Blindern, 0315 Oslo, Norway

Compiled 3:35am on May 16, 2022.

ABSTRACT

Context. Data from ground-based, high-resolution solar telescopes can only be used for science with calibrations and processing that require detailed knowledge about the instrumentation. Space-based solar telescopes provide science-ready data, easier to work with for researchers whose expertise is in the interpretation of data. Recently, data processing pipelines for ground based instruments have been constructed.

Aims. We aim to provide observers with a user-friendly data pipeline for data from the Swedish 1-meter Solar Telescope (SST), that delivers science-ready data together with the metadata needed for proper interpretation and archiving.

Methods. We describe the CHROMIS instrument briefly, including its (pre)filters, as well as recent upgrades to the CRISP prefilters and polarization optics. We summarize the processing steps, from raw data to science-ready data cubes in FITS files. We go into detail about calibrations and compensations for data imperfections. Misalignment of Ca II data due to wavelength-dependent dispersion is identified, characterized, and compensated for. We describe intensity calibrations that remove or reduce the effects of filter transmission profiles as well as solar elevation changes. We present REDUX, a new version of the MOMFBD image restoration code with multiple enhancements and new features. It uses projective transforms for the registration of multiple detectors. We describe how image restoration is used with CRISP and CHROMIS data. The science-ready output is delivered in FITS files with metadata compliant with the SOLARNET recommendations. Data cube coordinates are specified within the World Coordinate System (WCS). Cavity errors are specified as distortions of the WCS wavelength coordinate with an extension of existing WCS notation. We establish notation for specifying the reference system for Stokes vectors with reference to WCS coordinate directions. The CRISPEX data cube browser has been extended to accept SSTRED output and take advantage of the SOLARNET metadata.

Results. SSTRED is a mature data processing pipeline for imaging instruments, developed and used for the SST/CHROMIS imaging spectrometer and the SST/CRISP spectropolarimeter. SSTRED delivers well-characterized, science-ready, archival quality FITS files with well-defined metadata. The SSTRED code, as well as REDUX and CRISPEX are all freely available through git repositories.

Key words. Instrumentation: high angular resolution – Instrumentation: polarimeters – Methods: observational – Techniques: imaging spectroscopy – Techniques: image processing

1. Introduction

Scientists working with data from ground-based, high-resolution solar telescopes were for many years required to have detailed knowledge about the telescopes and instruments with which their data were collected. With the complexity of instruments and observing sequences developed during the last decades, this has become increasingly difficult. Only the home institutes of the instruments and a few other, strong groups were able to maintain the necessary knowledge.

Meanwhile, space-based solar telescopes have come with data pipelines that deliver well-characterized data, along with metadata that facilitate their interpretation. Such data have then been made available to researchers around the world through web-based virtual observatories with searchable databases, e.g., Hinode (Kosugi et al. 2007), IRIS (De Pontieu et al. 2014), and SDO (Couvidat et al. 2016). This has significantly increased the scientific use of those data.

In recent years, data pipelines also for the major ground-based telescopes have been made available to observers, making the production of science-ready data a matter of some training and adequate computer resources. This is a crucial development

for solar data from ground-based telescopes to have their scientific potential properly realized. Some of these pipelines are the IBIS Software Package (Criscuoli & Tritschler 2014) for the Interferometric BiDimensional Spectropolarimeter (IBIS); CRISPRED (de la Cruz Rodríguez et al. 2015, hereinafter referred to as the CRISPRED paper) for the CRisp Imaging SPectropolarimeter (CRISP); the ROSA data reduction pipeline (Jess & Keys 2017) for the Rapid Oscillations in the Solar Atmosphere instrument (ROSA); sTools (Kuckein et al. 2017) for the GRE-GOR Fabry-Pérot Interferometer (GFPI) and High-resolution Fast Imager (HiFI).

Working within the 2013–2017 EU FP7 SOLARNET project (Collados 2017), Haugan & Fredvik (2015) set out to define the metadata needed for the inclusion of ground-based solar data in future Solar Virtual Observatories (SVOs). This adds another set of requirements for the documentation, based on the expectation that data will be used without the observers being involved. Within the second SOLARNET project (2019–2022, EU Horizon 2020), Haugan & Fredvik (2020) have further developed these recommendations as they have been confronted with implementations in pipelines, primarily SSTRED and the pipeline

for the Spectral Imaging of the Coronal Environment instrument (SPICE; SPICE Consortium et al. 2020).

With the August 2016 commissioning of the CHROMospheric Imaging Spectrometer (Scharmer 2017) at the Swedish 1-meter Solar Telescope (SST), a data processing pipeline was needed. Like CRISP, CHROMIS is based on dual Fabry–Pérot interferometers (FPIs) in a telecentric mount and is also similar in the design in other aspects. It was evident that the CRISPRED code would be an excellent starting point, but much of the code had to be generalized to remove CRISP-specific assumptions about cameras, filters, data file formats, etc.

Inclusion of metadata according to the then recently formulated SOLARNET recommendations in CRISPRED required a more thorough rewrite. We decided to work in a new fork, dubbed CHROMISRED, so observers reducing CRISP data would not be disturbed by the ongoing developments. When the new code base was fully operational for CHROMIS, we re-implemented full support for CRISP data in it.

This paper describes SSTRED: the new, combined pipeline for the two imaging spectro(polari)meters CRISP and CHROMIS.¹ With it we aim to provide the complex “machinery” needed to process multi-instrument, multi-wavelength data from a ground-based solar telescope, as well as compensate such data for known imperfections and prepare for their use together with space-based data.

SSTRED is being developed in parallel to the development of SOLARNET recommendations for metadata, and includes multiple calibration and correction steps beyond the standard pixel bias and gain, alignment and destretching, and image restoration. SSTRED is therefore well placed to serve as a model for pipelines of future instruments.

SSTRED was under development 2016–2021 and features were added as late as in March 2021. A draft version of this paper has been available since April 2018 [arXiv:1804.03030v1], with a second version uploaded in July 2019. We describe the state of SSTRED in May 2021.

Combining data from multiple instruments with access to different wavelength bands greatly enhances the scientific analysis. Examples of such science are published by Leenaarts et al. (2018), Esteban Pozuelo et al. (2019), Buehler et al. (2019), Kuridze et al. (2019), Kianfar et al. (2020), Pietrow et al. (2020), Joshi et al. (2020), Rouppe van der Voort et al. (2021), and Bose et al. (2021), evidence of the utility of SSTRED-processed data. Rouppe van der Voort et al. (2017) and Vissers et al. (2019) present data that tap into an even more complex but also more powerful application of SSTRED-processed data, which includes the analysis of CRISP and CHROMIS data together with space-based data from IRIS. More of the latter can be expected as Rouppe van der Voort et al. (2020) have released an archive of CRISP and CHROMIS data that are registered with IRIS data.

We also describe updates to the auxiliary data-cube browsing program CRISPEX, as well as relevant details of the CHROMIS and CRISP instruments and other optics.

The organization of this paper is as follows. We first describe the instrumentation (Sect. 2) and give an overview of the data processing steps performed by SSTRED (Sect. 3) with references to the literature (in particular the CRISPRED paper, which is recommended reading for the interested reader) when possible. We then describe in detail aspects of the processing that are novel to SSTRED (calibration steps in Sect. 4 and image restora-

tion in Sect. 5). SSTRED output is rich in metadata, stored in accordance with the SOLARNET recommendations, as described in Sect. 6. We present updates to the CRISPEX data browser, relevant to exploring and analyzing the SSTRED science-ready output, in Sect. 7. We end with a discussion in Sect. 8. Some details about implementation are found in the Appendices.

2. Instrumentation

The optics of the SST (Scharmer et al. 2003) and its imaging setup are illustrated in Figs. 1 and 2, respectively. In the caption of the latter figure, acronyms are defined for many optical elements that are discussed in the following two subsections, with details about the CRISP and CHROMIS instruments.

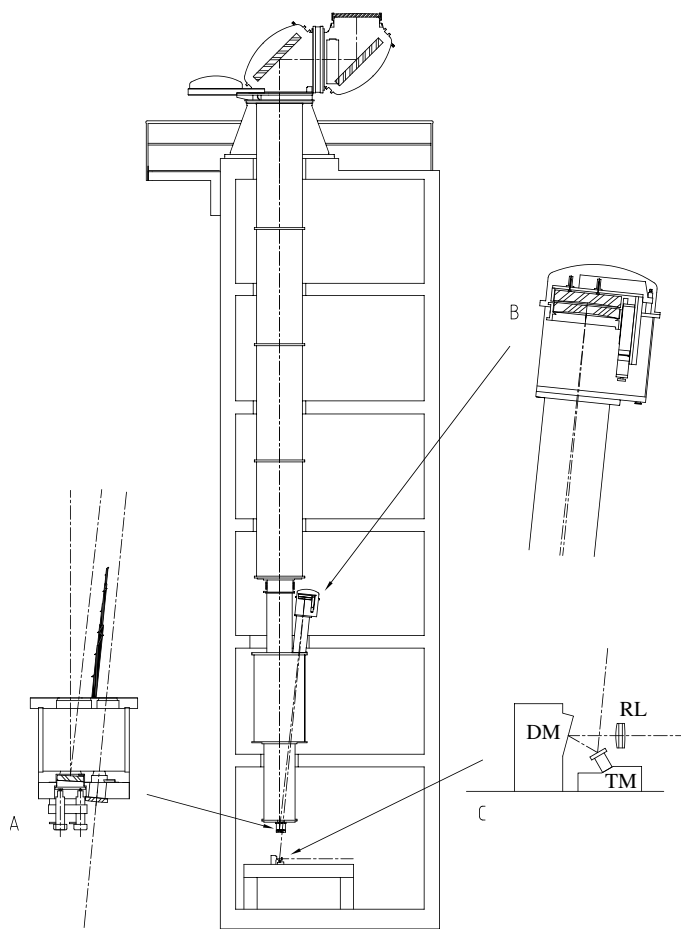


Fig. 1: Sketch of the SST (from Scharmer et al. 2003), from the 1-m lens, via the two alt-az mirrors, the field mirror on the bottom plate (inset A), the Schupmann corrector (B), the field lens and exit window (A), to the tip-tilt mirror (TM), deformable mirror (DM), and re-imaging lens (RL) on the optical table (C). The optical path continues in Fig. 2.

2.1. CRISP

The CRisp Imaging SpectroPolarimeter (CRISP) operates in light with $\lambda > 500$ nm, reflected by the DC into a red beam. Details about CRISP are given by Scharmer et al. (2008) and (with an emphasis on data processing) in the CRISPRED paper. Here follows a brief update.

¹ The names CRISPRED and CHROMISRED are retained as the modes of SSTRED used for the two instruments.

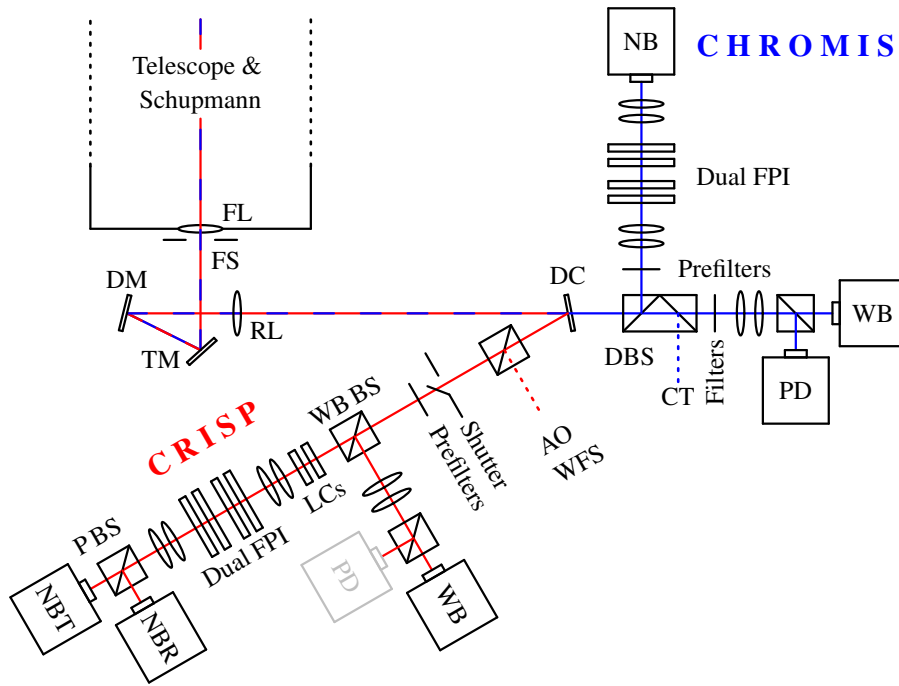


Fig. 2. Schematics of the setup used from the CHROMIS installation in August 2016 through the 2020 season. Acronyms: FL = field lens, FS = field stop, TM = tip-tilt mirror; DM = deformable mirror; RL = reimaging lens; DC = 500 nm dichroic beamsplitter; DBS = double beamsplitter, CT = correlation tracker; AO WFS = adaptive optics wavefront sensor; WB BS = wide-band beam splitter; FPI = Fabry–Pérot interferometer, LCs = liquid crystal modulators; PBS = polarizing beamsplitter, NB = narrowband, WB = wideband, NBT = NB transmitted, NBR = NB reflected, PD = phase diversity. White light enters the telescope from the top. It is split into a red and a blue beam at ~ 500 nm by the DC. Distances and angles do not correspond to the physical setup.

Before the 2015 season, new ferroelectric LCs (de Wijn et al. 2021) were installed as a polarimetric modulator, replacing the old nematic LCs. Because they occupy more space on the optical table, they were installed directly after the WB BS rather than in the old position before the PBS.

We have known since 2013 that the original CRISP prefilters manufactured by Barr have significant optical power, making the focus vary between the filters. This was compensated for by use of a variable focus on the DM, with the unfortunate consequence of leading to focus errors in the blue beam instead. In practice, this limited most CRISP observations to use prefilters that happened to have similar optical power or to not allow simultaneous blue data to all CRISP observations. New CRISP prefilters without optical power, made by Alluxa, were installed before the 2018 season.² Transmission profiles are shown in Fig. 3, see also Table 1.

The varying optical power caused a variation in image scale of up to several percent between some of the old CRISP prefilters. The image scale with the new filters agree to within $\sim 0.1\%$.

There are four Sarnoff CAM1M100 cameras for CRISP, but only three at a time have been used regularly. The fourth has been used as a spare but is no longer operational.

2.2. CHROMIS

The CHROMospheric Imaging Spectrometer (CHROMIS; Scharmer et al. in prep.; Scharmer 2006) is based on a dual FPI mounted in a telecentric setup, similar to CRISP but designed for use at wavelengths in the range 380–500 nm and currently without polarimetry. In particular, CHROMIS is optimized for use in the Ca II H and K lines, which are formed in the upper chromosphere, and the H- β line.

The blue light with $\lambda \lesssim 500$ nm is transmitted through the DC toward the DBS, that reflects most of the light to the narrowband (NB) beam and transmits the remainder to the wideband

(WB) beam (where it is again split between the CT and the two WB cameras). The DBS was designed to reflect 90% to the NB path but the current DBS does not reflect more than $\sim 60\%$. A new DBS with the proper splitting would improve the signal-to-noise ratio (SNR) in the NB and should be installed before a future polarimetry upgrade of the instrument.

The NB path goes through one of a set of filters mounted in a filter wheel, the filter characteristics are summarized in Table 2 and Fig. 4. These filters are all manufactured by Alluxa.

With the present set of prefilters, CHROMIS can be used in two wavelength regions. One region covers the Ca II H and K lines. Scanning through the wide Ca II lines and nearby continuum at 399 nm is done through five separate 3-cavity NB prefilters, while simultaneous WB data, used for context and supporting image restoration, are collected through a single WB filter with a wavelength between the H & K lines. The other region covers the H- β line, with WB data collected in the continuum to the blue of the line.

The design FWHM of the FPI NB transmission profile is 8 pm at the Ca II H and K lines and 10 pm at H- β . However, the measured profile width in Ca II is estimated to ~ 13 pm (Roupe van der Voort et al. 2017), which has been traced to a mismatch in the etalon reflectivities.³

The WB re-imaging system provides a telecentric beam with the same focal ratio as the one of the CHROMIS FPIs. It provides an *anchor* object for image restoration, see Sect. 5. The PD camera collects WB data approximately 1 wave out of focus to further facilitate image restoration with Phase Diversity.

The Ca II H&K WB filter has been in use from the start, providing a photospheric image that works very well for on-disk image restoration. However, it gives very little signal outside the limb without saturation on the disk. Kuridze et al. (2019) managed to restore coronal loops but it has been clear that a WB filter with better visibility of fine structure outside the limb would be an advantage. The Ca II H core WB filters were installed in Au-

² The 587.66 nm He D3 filter was installed already in 2016, but it belongs to the new batch of Alluxa filters with no optical power.

³ The profile width depends on the reflectivities in the high-resolution etalon, see Sect. 2.1 and Fig. A.1 in the CRISPRED paper.

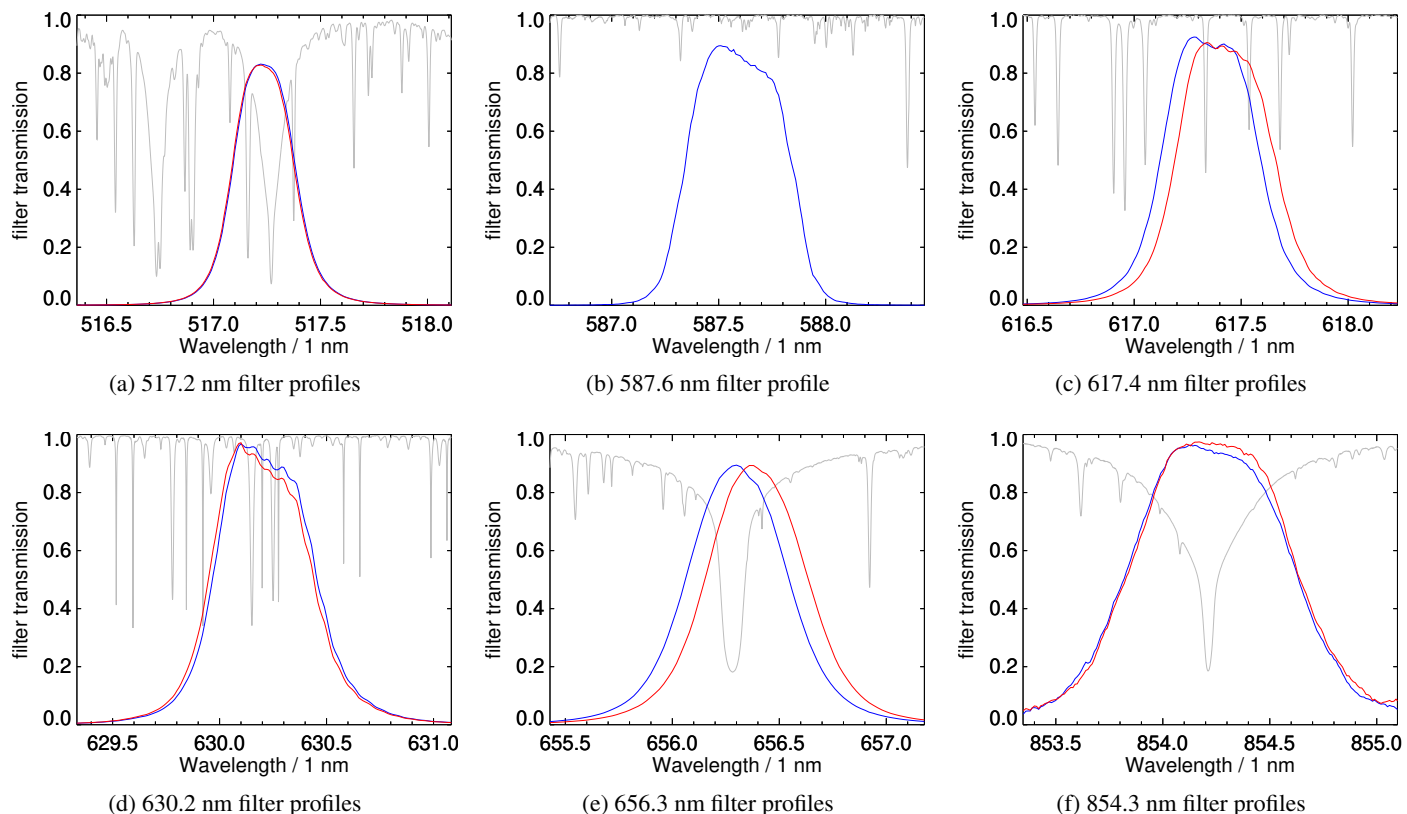


Fig. 3: CRISP prefilter transmission profiles as measured by the manufacturer. The blue and red curves for each wavelength band (except for the 587.6 nm filter) correspond to two filters, one of which was installed before the 2018 season. The grey lines represent the average disk center atlas spectrum, normalized to the continuum. See also Table 1.

Table 1: table

CRISP prefilters installed 2018.

Main diagnostic [nm]	Unit #	CWL [nm]	FWHM [nm]	T_{peak}	PC
Mg I	1 (7)	517.24 (517.23)	0.32 (0.32)	0.83 (0.83)	
He D3	9	587.66	0.54	0.90	✓
Fe I	(6) 9	(617.36) 617.43	(0.49) 0.50	(0.92) 0.91	✓
Fe I	(9) 10	(630.21) 630.19	(0.50) 0.50	(0.97) 0.97	✓
H- α	(1) 10	(656.30) 656.40	(0.52) 0.53	(0.89) 0.89	
Ca II	(7) 10	(854.22) 854.23	(0.84) 0.83	(0.96) 0.97	✓

Notes. The CWL (center wavelength) and FWHM values are measured from the profiles plotted in Fig. 3. PC: Calibrated telescope polarization model exists.^a The numbers in parentheses correspond to filters not currently installed in the CRISP filter wheel. Compare Table A.1 in the CRISPRED paper.

^a There have been problems with fitting the telescope model to calibration data for the 517 nm filter. Until proper calibrations can be made, we are using the model for the old 525 nm filter (see the CRISPRED paper).

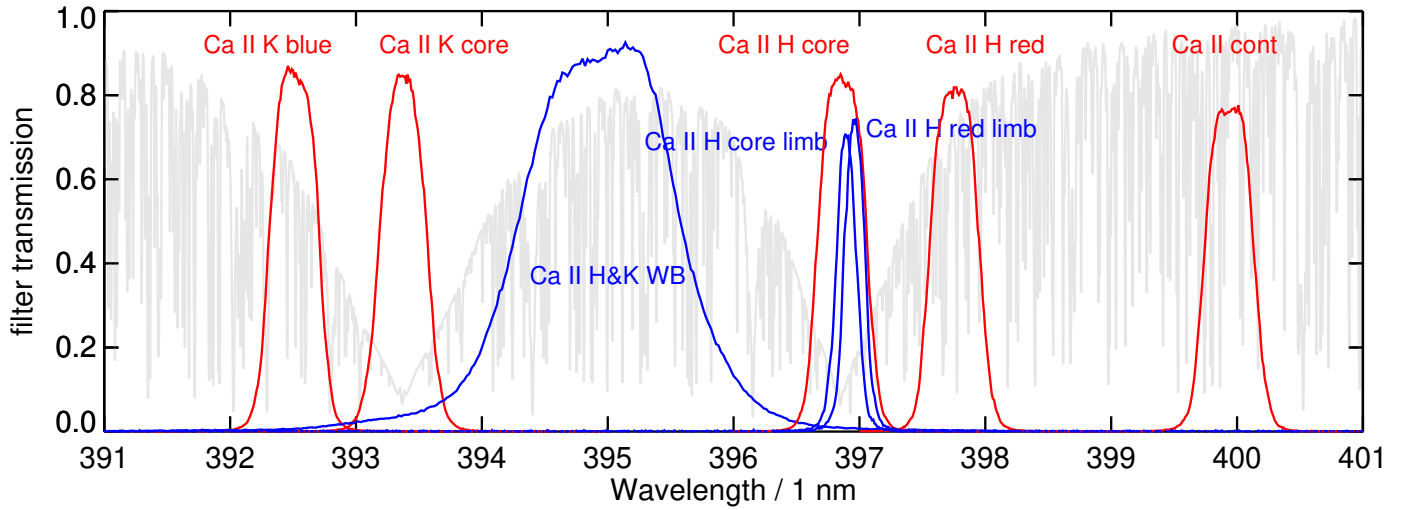
gust 2020, details about their use will be provided in the forthcoming CHROMIS paper.

All three cameras are Grasshopper3 2.3 MP Mono USB3 Vision (GS3-U3-23S6M-C) cameras, manufactured by PointGrey. They are equipped with Sony Pregius IMX174 globally shuttered 1920×1200-pixel CMOS detectors with 5.86 μm pitch. These cameras are synchronized electronically so there is no need for an external shutter as in CRISP. The plate scale was $\sim 0''.038/\text{pixel}$ during the 2016–2020 seasons, measured in pinhole array images using a pinhole spacing of $5''.116$ (see the CRISPRED paper, Sect. 3.3).

3. Overview of SSTRED processing

This section gives an overview of the processing steps for reducing CRISP and CHROMIS data with SSTRED. See Appendix A for notes on the pipeline code.

The processing divides naturally into steps performed before image restoration (with multi-object multi-frame blind deconvolution, MOMFBD), the MOMFBD processing itself, and post-MOMFBD steps.



(a) Ca II filter profiles

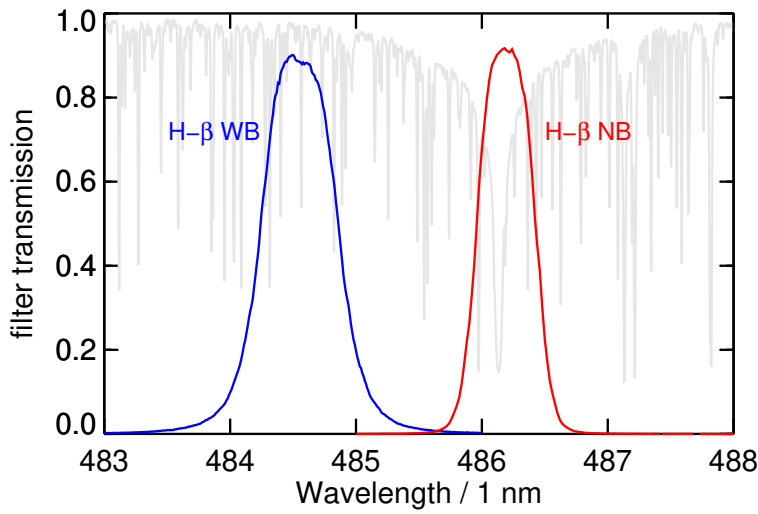

(b) H- β filter profiles

Fig. 4: CHROMIS filter transmission profiles (normal incidence). Red lines: NB pre-filters. Blue lines: WB filters. The filter profiles shown are measured in the center of the filter by the manufacturer. The FPI profiles are not wide enough to plot here. The grey lines represent the average disk center atlas spectrum, normalized to the continuum. See also Table 2.

Table 2: table

CHROMIS filters.

Wide-band filters				NB prefilters			
Wavelength band	CWL [nm]	FWHM [nm]	T_{peak}	Wavelength band	CWL [nm]	FWHM [nm]	T_{peak}
Ca II H&K WB	395	1.32	0.9	Ca II K blue Ca II K core Ca II H core Ca II H red Ca II continuum	392.52	0.41	0.86
Ca II H red limb WB	396.96	0.18	0.74		393.41	0.41	0.8
Ca II H core limb WB	396.90	0.18	0.71		396.88	0.41	0.8
					397.74	0.41	0.83
					399.04	0.42	0.76
H- β WB	484.55	0.65	0.9	H- β NB	486.22	0.48	0.92

Notes. CWL = center wavelength at normal incidence, T_{peak} = peak transmission as given by the manufacturer. See also measured transmission profiles in Fig. 4. The curly brackets indicate that any of the Ca II WB filters can be combined with any subset of the Ca II NB prefilters.

3.1. Pre-MOMFBD

The first step in processing CRISP and CHROMIS data for a particular observing day is running a setup script, that locates and analyzes the directory tree with the day's observed data, identifying science data as well as the various kinds of calibration data. A work directory (one per instrument) is created, where

a configuration file and an IDL⁴ script with the recommended processing steps are written.

Most calibration data are collected as bursts of images with the same settings and exposure times as the science data. These bursts are then summed, resulting in calibration data where noise and (when relevant) imprints from granulation are reduced. Such

⁴ Interactive Data Language, Harris Geospatial Solutions, Inc.

summing is done for dark frames, flat fields, pinhole array images, polarimetric calibrations. While summing, statistics are calculated. This allows checking for outliers and removal of suspicious frames. Flats and pinholes for the near-IR wavelength bands 7772 and 8542 Å recorded with CRISP are corrected for back scatter. See Sect. 4.2 of the CRISPRED paper for details.

Based on the summed polarimetric calibration data, modulation matrices are then calculated for each CRISP pixel. See Sect. 4.1 of the CRISPRED paper.

The geometrical transform needed to align images from different cameras are estimated by a calibration step involving pinhole array images. We describe a procedure for doing this in Sect. 4.1, that is improved with respect to the procedure described in Sect. 3.2 of the CRISPRED paper.

The FPI cavity errors are measured from the summed flat fields. See Sect. 4.2 below.

The intensities registered by the detectors are affected by the transmission through the atmosphere, the telescope, other optics including in particular the prefilters, as well as the quantum efficiency (QE) of the detectors. These effects depend on both time and wavelength. We measure the effects from calibration data as described in Sects. 4.4.1 and 4.4.2 below.

3.2. MOMFBD

The MOMFBD image restoration is done outside of IDL, details in Sect. 5. SSTRED uses a recent fork of the MOMFBD code written by van Noort et al. (2005), with several essential new features. The new code, REDUX, is described in Appendix A.3.

The MOMFBD processing includes image remapping based on pinhole calibration. This step aligns images from different cameras, see Sect. 4.1.

Back scatter correction for CRISP Sarnoff cameras in near IR wavelengths as described in Sect. 4.2 of the CRISPRED paper.

3.3. Post-MOMFBD

The post-MOMFBD steps assemble the MOMFBD-restored images into science-ready data cubes with metadata. The cubes have dimensions $[N_x, N_y, N_{\text{tun}}, N_{\text{pol}}, N_{\text{scan}}]$, where N_x and N_y are the spatial dimensions, N_{tun} is the number of wavelength tuning positions, N_{pol} is the number of polarization states (4 for Stokes data, 1 otherwise), and N_{scan} is the number of scans through the line. The physical coordinates are two spatial coordinates, the wavelengths, the polarization states, and the temporal coordinates. They are not strictly equivalent to the pixel coordinates. The spatial coordinates, solar longitude and latitude, vary with time (due to the solar rotation), and the time coordinate is advanced both while tuning and from scan to scan. This is specified in the metadata using the World Coordinate System (WCS), see Sect. 6.3.

The following steps are performed on the restored NB images, to produce a science-ready data cube:

- For polarimetric CRISP data: demodulation of images in four LC states to Stokes components. See Sect. 4.1 in the CRISPRED paper as well as Selbing (2005) and van Noort & Rouppe van der Voort (2008).
- Removal of periodic image artifacts in polarimetric data. See Sect. 4.3
- For CHROMIS Ca II data: correction for time-variable misalignment due to chromatic dispersion in the atmosphere and in the telescope. See Sect. 4.5.

- Correction for residual warping from anisoplanatic effects between NB images with different tuning and/or polarimetric states. See Sect. 5.4.
- Compensation for field rotation caused by the alt-az mount of the telescope. See Sect. 4.7.
- For cubes with multiple scans, geometrical alignment and destretching needed to make the transition from scan to scan smooth. See Sect. 4.6 in the CRISPRED paper.
- For polarimetric CRISP data: removal of polarimetric crosstalk. See Sect. 4.6.
- Spectral intensity scaling to compensate for prefilter transmission profiles and to get correct units by use of the prefilter calibration described in Sect. 4.4.1.
- Temporal intensity scaling to compensate for changes in solar elevation. See Sect. 4.4.2
- Finalize. A final adjustment of metadata to bring cubes made with earlier versions of SSTRED up to SOLARNET compliance. Statistics (see Sect. 6.4) and checksum calculations.
- Archiving and export. Make thumbnail images and context videos. Upload science data cubes to local disks accessible from the internet. Upload metadata to databases (local and SVO).

3.4. SVO

As the last (optional) steps in the post-MOMFBD processing, we upload the science data cubes to a web-accessible disk area at Stockholm University.

We also upload the metadata for the science-ready data to an SVO. At this point we specify the SOLARNET keywords RELEASE (a date after which the data are released to the community) and RELEASEC (a comment describing the data policy and/or a link to more information about such policy).

Presently we use the prototype SVO, hosted by the Royal Observatory of Belgium, developed by Mampaey et al. (2017) in the first SOLARNET project. We expect to move to the production SVO, developed by the same group (Mampaey et al., in prep.) in the second SOLARNET project, when it is operational. The SVO facilitates searches in the metadata and can serve URLs for data downloads from the Stockholm servers. These search-and-download operations can also be done by use of IDL scripts. The server is aware of the RELEASE keyword and knows to issue a password challenge if the release date is in the future.

4. Calibrations

Here we describe calibrations that were not mentioned in the CRISPRED paper or are done differently in SSTRED.

4.1. Camera alignment

Optical setups that utilize beamsplitters, filters, and lenses are never perfectly stable in terms of alignment. So we need to routinely calibrate the alignment of the cameras, separately for each prefilter. The tuning of the Fabry–Pérots and the changes in the polarization states of the LCs in practice turn out to not have a significant effect, so we average the measurements over those.

The co-alignment of the cameras is measured by use of images of a pinhole array target mounted in the Schupmann focus, directly after the FS. This process is described by van Noort et al. (2005) and in Sect. 3.2 of the CRISPRED paper, although we have changed some aspects of this calibration.

The new method fits a generic transformation matrix to the relative pinhole positions as measured first by locating the peaks

and then by maximizing the cross-correlation between subimages with the individual pinhole images. Previously, relative positions were measured as wavefront tilt components with the MOMFBD program, one hole at a time.

Another change is in how the results of the calibration is represented. Before, field-dependent shifts in the two axis directions were stored as detector-pixel maps of offsets in X and Y. This format can represent very general geometric deformations but were in practice only used for global shifts (small ones, large ones represented by ALIGN_CLIPS), image scale differences, skew and field rotation. When the MOMFBD program had read a subfield in the anchor WB image it would get the matching subfield in another camera/channel by looking up the X and Y shifts for the center position of the anchor camera and 1) applying the rounded offsets to the pixels coordinates to read out and 2) adding the subpixels remainders of the offsets to the wavefront tilt terms of the channel.

This scheme has problems near the edges of the field of view. This is mostly due to the fact that the images are clipped before the offsets are applied. This leads to values of pixels near the corners being unnecessarily undefined (in practice, filled with zeroes) if there is even a slight rotation, or scale difference, between the cameras. In addition, the shifts are not accurately described by a quadratic surface near the edges (which the old calibration assumes). The calibration itself was also not very robust with respect to larger rotation misalignment between cameras. The new method, on the other hand, can handle arbitrary rotations and scale differences, and can also be used to align CRISP and CHROMIS images.

The new method consists of determining the *projective transforms* (see, e.g., Hartley & Zisserman 2000) relating each channel to the reference channel in the form of a 3×3 matrix,

$$H = \begin{bmatrix} h_{00} & h_{01} & h_{02} \\ h_{10} & h_{11} & h_{12} \\ h_{20} & h_{21} & 1 \end{bmatrix}, \quad (1)$$

acting on the projective coordinate vector, $[x, y, 1]^T$, followed by a normalization to maintain unity in the third element. The top-left 2×2 block of H encodes rotation, magnification and mirroring, h_{02} and h_{12} are translations in x and y (i.e. the top 2 rows of the matrix make up an *affine transform*) and the elements h_{20} and h_{21} are responsible for perspective skew and keystone effects. A simple sanity-check for the SST setup is that h_{00} and h_{11} should be close to +1 or -1, h_{02} and h_{12} should be within a few tens of pixels from 0 (or from the detector size, in case of mirroring), and that h_{20} and h_{21} should be tiny ($\sim 10^{-5}$).

Besides the advantages in accuracy and efficiency of the calibrations, and alignment during MOMFBD, there are some additional bonuses. E.g., inverse or composed mappings are trivial matrix operations. Many software libraries (such as OpenCV) can be used to manipulate images based on these transformation matrices.

4.2. Cavity errors

CRISP and CHROMIS are based on dual FPIs, mounted in a telecentric configuration. The central wavelength of the FPI transmission profile can be tuned to different wavelengths by changes in the separation of the etalon cavities. There are deviations from the nominal tuning wavelengths caused by very fine spatial variations, δD , in the cavity, D , between the two plates of an etalon. Because the etalons are located near the focal plane, the variation over the etalon surfaces translate to variations over

the FOV: the passband is not centered at exactly the same wavelength over the entire FOV.

These cavity errors, interpreted as distortions in the wavelength coordinate, λ , through $\delta\lambda = \delta D \cdot \lambda/D$, have to be taken into account when interpreting the data, in particular when fitting CRISP and/or CHROMIS data to models of the solar atmosphere.

4.2.1. Measurement

The method for measuring the cavity errors in CRISP from flat field data was developed by Schnerr et al. (2011) and is also described in Sect. 4.3 of the CRISPRED paper. It is based on an assumption that the pixels in a scan all show the same spectrum, and fits a pixel-map of wavelength shifts. For this a sufficiently well sampled line, including slopes in both directions, is needed. We use the same method for CHROMIS, see Fig. 5 for cavity errors measured for CHROMIS.

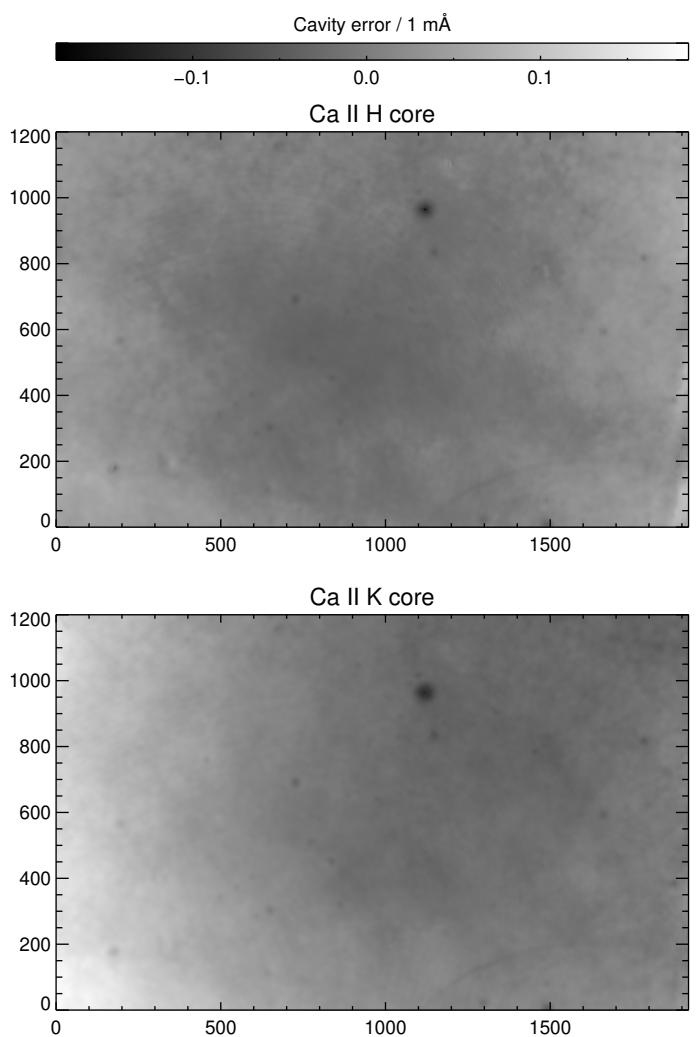


Fig. 5: Cavity error of the high resolution CHROMIS etalon through the Ca II H and K core prefilters as measured with data from 2016-09-19. Mapping the associated wavelength shift over the 1920×1200-pixel NB detector.

The tuning of the CRISP and CHROMIS etalons is controlled digitally, with step sizes that were calibrated when the instruments were installed. One might worry that the etalon sep-

ation could change with tuning, like recently measured by Greco et al. (2019) in a laboratory setup. If the three piezo stacks that control the cavity width do not move by the same amount, we would get a time-variable linear component (tilt) in the cavity separation. However, the accuracy of the tuning control is estimated to ± 0.0005 mÅ/du for CRISP and ± 0.01 mÅ/du for CHROMIS (P. Sütterlin 2020, priv. comm.).

While the calibration is good enough that tilt *variations* with tuning are negligible within the tuning range of a prefilter, the cavity errors still do have a tilt component. The tilt component depends on the settings of parameters related to the piezos that control the gap when tuning, and those parameters are set by daily calibrations that are independent for each prefilter. So for CHROMIS Ca II, where multiple prefilters are used in a single scan, the tilt (and possibly other low-order components) of the gap varies from one prefilter to another.⁵ Compare the cavity maps for the two Ca II core filters in Fig. 5.

The Ca II H and K wing filters have so far hardly been used but it should be possible to calibrate them using some of the blends in the wing filter pass bands. It should be possible also for the Ca II continuum filter, although it is not needed as long as it is not used to scan through any of the lines within its passband.

See Appendix B for how the cavity errors are stored as distortions to the WCS wavelength coordinate.

4.2.2. Flat fielding

When observations are made in the parts of spectral lines where the intensity changes rapidly, the cavity error wavelength shifts cause a spatial imprint in the intensities of both data and flats. The wavelength shifts cause intensity changes that are not accounted for in the monochromatic image formation model assumed by MOMFBD. This can cause suboptimal solutions for the wavefronts (i.e., the PSFs) in the image restoration step, because of mismatches with the image formation model that assumes quasi-monochromatic data. For polarimetric observations, the time-dependent telescope polarization also has an effect on the flat fields. Also, deconvolving large discontinuities in the cavity errors can cause artifacts in the MOMFBD output. For these reasons, Schnerr et al. (2011) developed a method for taking all this into account

Science data is often collected in areas where the spectrum varies with both time and position in the FOV and is quite different from that of the quiet Sun, where flat field data is collected. The CRISPRED paper (see their Sect. 3.1) improved upon the procedure by Schnerr et al. (2011) to take also this into account. This is what is used for CRISP data in SSTRED.

The cavity errors of CHROMIS are both smoother and smaller than those of CRISP. CHROMIS cavity errors are ~ 0.1 mÅ (see Fig. 5) while CRISP cavity errors are ~ 10 mÅ (see Fig. 4 of the CRISPRED paper). Therefore, for CHROMIS we have found that the faster method by Schnerr et al. (2011) is sufficient.

4.3. Periodic artifacts

Polarimetric CRISP datasets often show periodic artifacts in the Stokes Q , U , and V components, in particular U and V . A sample U image with such artifacts is shown in Fig. 6(a). With dominating high-contrast features such as sunspots in the FOV,

⁵ This effect could have been reduced by sending control signals to each piezo stack individually. Sending a single control signal to all three is needed for fast scans.

it is difficult to separate the signal from the artifact. However, the same artifact is visible in the polarization calibration (polcal) image data. As polcal data are always collected in regions with quiet Sun, the offending spatial frequency can quite easily be found manually in the 2D power spectrum of sums of polcal images. A sample image is shown in Fig. 6(b). This spatial frequency is then removed from the Stokes images by use of a two-dimensional notch filter, the result of which is shown in Fig. 6(c).

Similar Fourier filtering was implemented in CRISPRED but it was left to the user to actually construct the filter. Díaz Baso (2018, his Fig. 2.19) and (Pietrow et al. 2020, their Fig. 2) implemented their own similar corrections before the filter described here was included in SSTRED.

The artifact pattern seems stable over years of observations but is measured independently for each new day of observations. Note that a pattern with the same period and direction is visible also in the modulation matrix components. Our first thought was to apply the notch filter to this matrix before demodulating the data. However, this turned out to make the artifacts worse.

A close inspection of Fig. 6(c) shows cross-talk from Stokes I as a weak granulation pattern imprint outside the spot (in particular in the top part), see Sect. 4.6 for how this is removed.

4.4. Intensity calibration

4.4.1. Spectral intensity-calibration

In order to characterize the wavelength-dependent instrument response in our observations, we use the Hamburg disk center atlas spectrum (Neckel 1999; Brault & Neckel 1987) as a reference. We degrade the atlas spectrum by convolution with a theoretical FPI transmission profile. We then estimate the parameters in a model prefilter profile by fitting the degraded atlas spectrum to quiet Sun data collected at disk center. The prefilter model is a Lorentzian multiplied with an anti-symmetric polynomial,

$$\bar{P}(\lambda, p_0, \dots, p_6) = \frac{p_0}{1 + \left(2 \frac{\lambda_c - p_2}{p_3}\right)^{2p_4}} \cdot (1 + p_5 \lambda_c + p_6 \lambda_c^3) \quad (2)$$

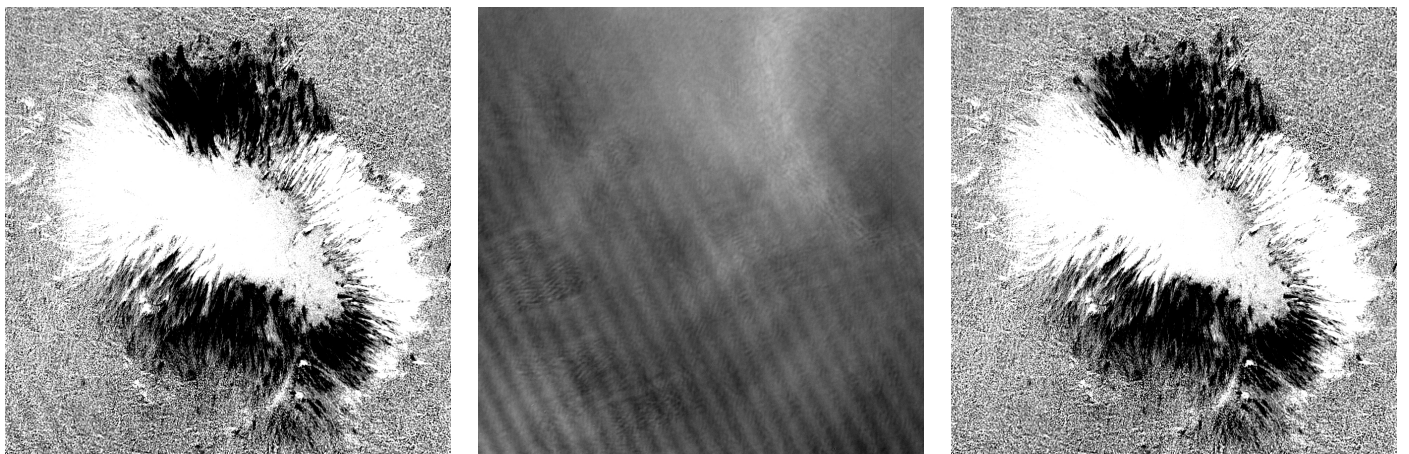
where

$$\lambda_c = p_1 + (\lambda - \text{CWL}) \cdot p_7. \quad (3)$$

The parameters have the following effects on the fit: p_0 is a scale factor from counts to the units of the atlas; p_1 shifts the wavelength scale to align the spectral lines in the data with those in the atlas spectrum; p_2 is a shift of the CWL of the prefilter; p_3 is the FWHM of its transmission profile; p_4 is the number of cavities in the filter; the polynomial with parameters p_5 and p_6 represent asymmetries in the profile as well as in other wavelength-dependent effects⁶ on the number of collected photons; the seldom used p_7 stretches the wavelength grid. The Lorentzian represents the prefilter transmission profile, where not constraining the number of cavities to be an integer accounts for some deviations from an idealized filter.

Fig. 7 shows examples of these fits for Ca II K and H- β . The derived prefilter curves are also plotted along with the fits in this figure.

⁶ Such as the quantum efficiency of the detector as well as the transmission of other optics and the atmosphere.



(a) Stokes U component, sunspot saturated to emphasize artifacts in the lower left corner.

(b) The polarization calibration image that the Fourier filter is based on.

(c) Fourier filtered U component, the artifacts removed.

Fig. 6: Removal of periodic artifacts in polarimetric data. The sample CRISP Fe I 6302 Å, -210 mÅ from line core, data were collected on 2019-05-10 at 09:07 UT. The FOV shown is $53''$ squared.

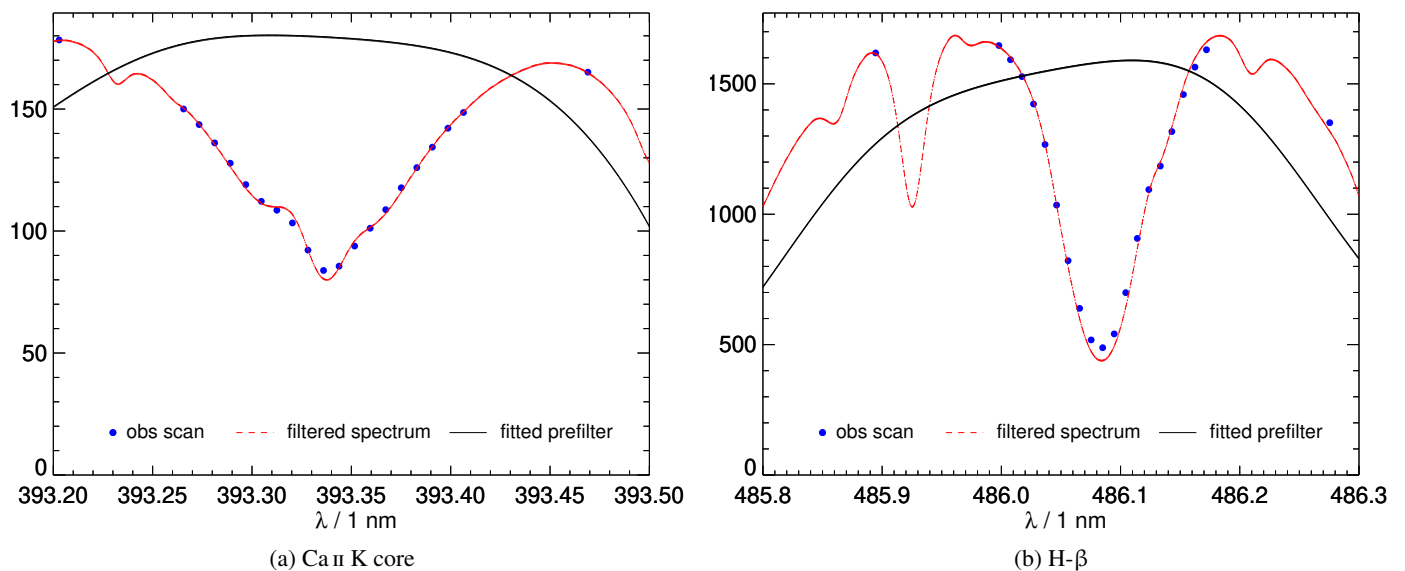


Fig. 7: Sample diagnostic plots from the spectral intensity-calibration. The scan intensities are plotted in counts while the “fitted prefilter” transmission is plotted in arbitrary units.

As described in Sect. 4.5 of the CRISPRED paper, the fitted profile (defined by parameters p_0 and p_2-p_6) is used to compensate science data for the wavelength-dependent response of the instrument and to convert the camera *counts* to intensity in SI units ($\text{W m}^{-2} \text{Hz}^{-1} \text{sr}^{-1}$). In addition, p_1 is used to adjust the wavelength coordinate from the one set by the instrument calibration made each morning at the telescope.

4.4.2. Temporal intensity-calibration

The spectral intensity calibration in the previous subsection is used to remove the effect of the prefilter transmission profiles and scale intensity counts to SI units. However, because of variations in solar elevation and the amount of dust in the line of sight, this conversion is really only valid for the time the calibration data were collected.

Our previous approach to correcting for this was to apply a correction factor that is the ratio of median WB intensities of

the individual scan and that of the calibration data. This compensates for changes in elevation and dust, but has the drawback that it also removes the inherent intensity variations from solar disk center to limb. A better intensity calibration would need a similar measured intensity ratio, but with both WB intensities obtained at disk center.

The present default calibration procedure is based on a polynomial fit to WB intensity data collected throughout the observing day. It doesn’t matter if the data are science data or flats, as long as they are collected near disk center⁷ and temporally span the entire period of observations. We are using the median intensity so the procedure can tolerate science data obtained from active regions, as long as the FOV is not dominated by large sunspots or faculae. Sample data for both CRISP and CHROMIS

⁷ It might be possible to relax the requirement that these data are collected near disk center by correcting the intensities for limb darkening using measurements by, e.g., Neckel & Labs (1994) or Neckel (2005). However, this is not implemented at this point.

are shown in Fig. 8. The data illustrate the decrease in extinction toward the red wavelengths, to essentially no effect in the IR. By default, second order polynomials are used for the fit (first order if there are only two data points). Other fit functions can be specified if needed.

Figure 9 shows the effect of the corrections over two morning periods of observations. For the disk center data in Fig. 9(a), the uncorrected intensities show the variation with solar elevation, similar to the WB calibration curve. The corrected intensities show much smaller temporal variation, crossing the uncorrected curve at the time the spectral intensity-calibration data were collected. This holds for both the old and the new correction. In Fig. 9(b) we show a similar plot where data were collected during two center-to-limb scans. The disk center intensities are like those in Fig. 9(a): following the increase with elevation for the uncorrected data, and are essentially identical for the two correction methods. The variations with μ are removed from the “old” method data (except very near the limb, an effect of the FOV including a gradient toward the limb as well as off-limb darkness), but preserved with the “fit” method.

In the new procedure we have also implemented a correction for varying exposure time. This was not necessary in CRISPRED as CRISP is operated with a constant rotating-shutter speed. The exposure time of CHROMIS can easily be changed, e.g., when the target is moved from disk center to limb.

For data sets consisting of multiple scans, the old method corrects also for rapid variations in intensity that would be unaccounted for if the ratio of fitted WB intensities alone were applied as for the individual scans. Therefore, the “fit” correction takes into account the scan-to-scan variations in WB mean values. This results in corrections that remove the rapid variations, see sample results in Fig. 10.

We have implemented this step so that the new procedure is used by default but for data not temporally spanned by WB disk center data, it will fall back to the old method. See Sect. 4.4.2 for how the metadata of the cube includes information about which version of this step was actually performed.

4.4.3. Residual intensity variation

After the two intensity calibrations described in Sects. 4.4.1 and 4.4.2, Ca II continuum data still show systematic residual intensity variations. The 1% drop in intensity over the 30 min data collection interval in Fig. 10 (common to both methods) is consistent with the ~5% intensity drop over 2.5 h shown in Fig. 9.

The WB and NB continuum passbands are separated by ~5 nm and the gradient in the extinction wavelength-dependence is large around 400 nm. The effect can be replicated qualitatively with Rayleigh scattering and the semi-empirical expression for relative air mass as a function of zenith angle by Kasten & Young (1989), although not quantitatively well enough for an accurate correction.

We also found a systematic residual time-dependent variation in the ratio of intensities in the K line core and the continuum (separated even more in wavelength) in the same data sets (not shown).

4.5. Time-variable alignment

MOMFBD-restoration, together with the pinhole calibration described in Sect. 4.1, usually delivers images recorded at different wavelengths that are very well aligned. However, the wavelength range of scans involving multiple Ca II prefilters can extend over

more than 7 nm⁸ (see Fig. 4), which makes misalignment caused by wavelength-dependent dispersion significant.

The misalignment can be measured by use of cross-correlation of H&K WB and continuum data, which are both formed mostly in the photosphere. Figure 11 shows such measurements made with raw data collected during two morning hours. The misalignment is time-dependent and there are two components, one of which varies with telescope elevation in a way that suggests atmospheric dispersion. The other component is periodic and we found that the period matches that of the temperature of the telescope bottom plate, also shown in Fig. 11. The periodic variation was traced to an air conditioning unit that switched on/off at regular time intervals. Our working hypothesis for the periodic component is that the temperature variations have a minute effect on the alignment of the field mirror that reflects the SST beam to the Schupmann corrector (see Fig. 1, inset A) or within the corrector itself. The alignment of the Schupmann corrector has a wavelength dependent dispersion effect (Scharmer et al. 2003).

Regardless of the source of the dispersion, we have measured the misalignment not only with WB and continuum but also with images in the Ca II K blue wing and Ca II H red wing (formed at similar height in the solar atmosphere) and found that it varies linearly with wavelength over the relevant range.

SSTRED includes a procedure for measuring and correcting the misalignment of the MOMFBD-restored Ca II scans. The process needs to be repeated for each scan because of the temporal variations. The misalignment between the WB and NB continuum images is measured by cross-correlation in the MOMFBD-restored data. The misalignments at the Ca II H wavelengths are then calculated by linear interpolation between the WB 395 nm and the NB continuum 399 nm. Similarly, linear extrapolation gives the misalignment at the Ca II K wavelengths.

Because the cross-correlation measurements depend on the data quality, they are smoothed with a method that ignores outliers and weights data points with respect to image RMS contrast. The variations around the smoothed line (disregarding the low-contrast outliers) suggest that the precision is a few tenths of a pixel, see Fig. 12.

Correcting this misalignment after MOMFBD restoration is much easier and less time consuming than doing it in the raw data. The misalignment is only a few pixels, small in comparison to the MOMFBD subfield size. The MOMFBD assumption of a common wavefront in WB and NB is therefore not significantly violated.

4.6. Polarimetric cross-talk

The telescope polarization model limits the accuracy of the demodulation. In the resulting Stokes cubes, there is cross-talk between the components. Due to the larger numbers in the I component compared to the differential Q , U , and V components, the most significant cross-talk is from I to the other components. This is corrected for similarly to the procedure used by Sanchez Almeida & Lites (1992).

If the field of view is free from polarization signal, any structures that match I in the differential components are cross-talk and the rest is noise. With this assumption and $X \in \{Q, U, V\}$, the correction for the X component can be written as

$$X \leftarrow X - w_X \cdot I \quad (4)$$

⁸ As a comparison, the wavelength ranges of scans through H- β and any the CRISP lines are typically less than 1 nm.

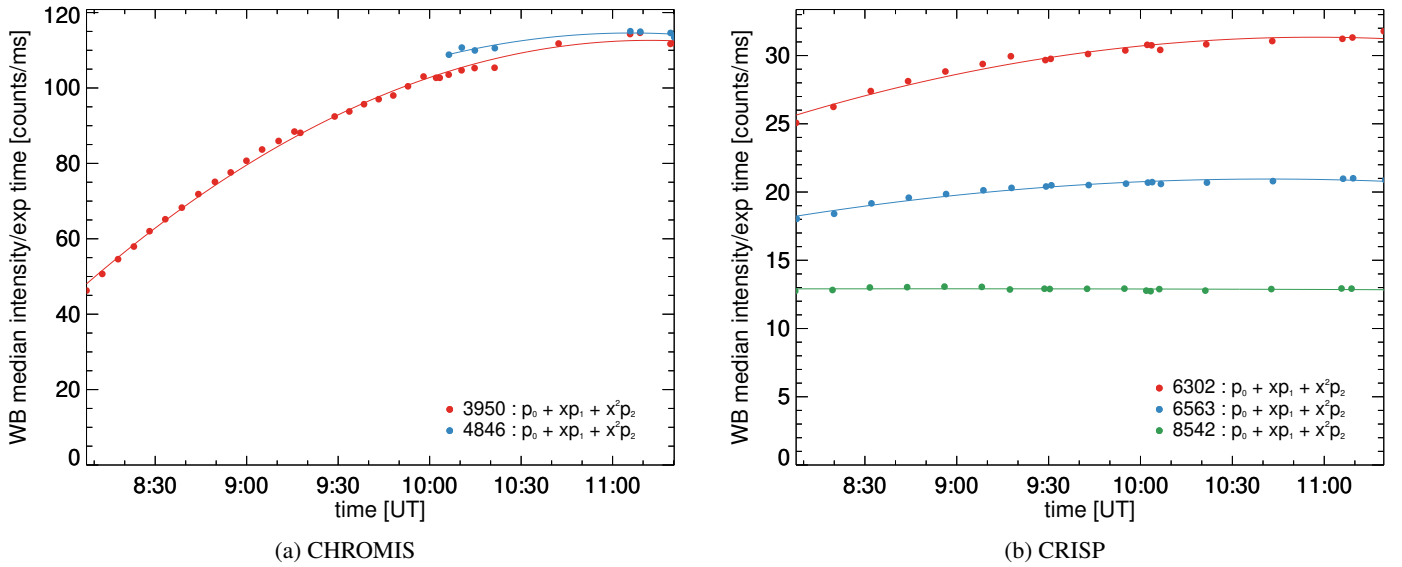


Fig. 8: Disk center median WB calibration intensities from 2016-09-19. Prefilter wavelength bands in Å as indicated in the legends. The solid lines are fits to second order polynomials as shown in the legends.

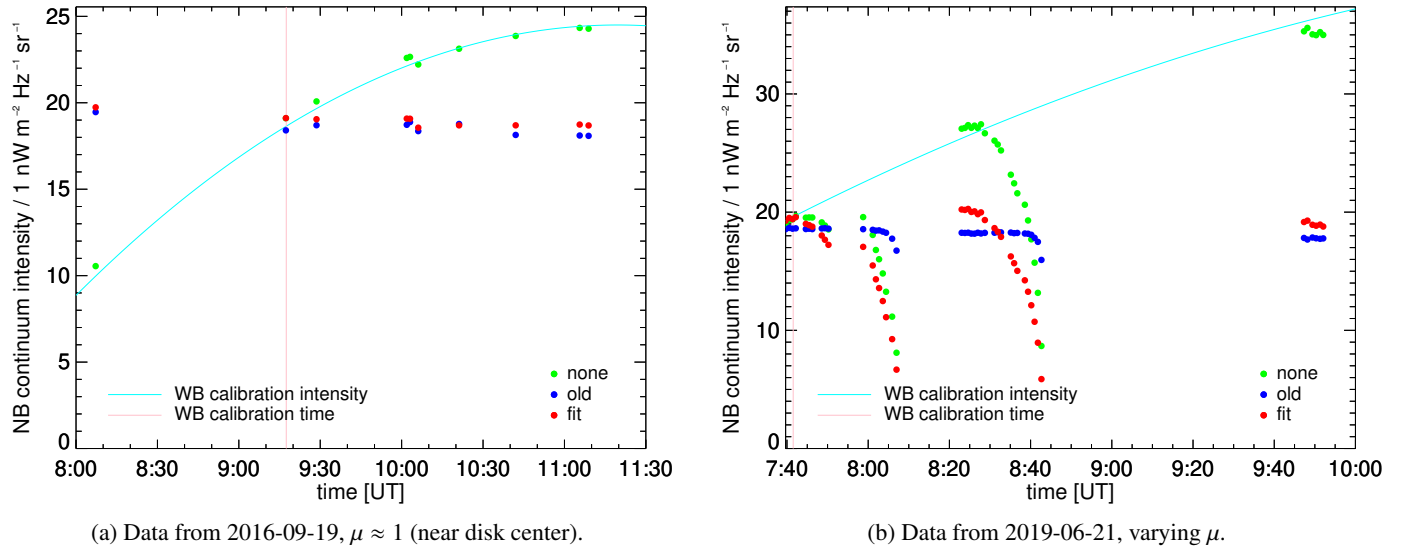


Fig. 9: CHROMIS Ca II NB continuum (median) intensities of restored data (individual scans), with and without temporal correction as indicated in the legends. The WB calibration curves are the fit functions (shown in Fig. 8(a) for the 2016-09-19 data), scaled to approximately match the disk center continuum intensities.

where the weight w_X can be estimated with a least-squares fit to the data in one or a few tuning states in (or as close as possible to) the continuum. We mask any spots, pores or other areas where a significant magnetic field can be expected and calculate

$$w_X = \langle I, X \rangle / \langle I, I \rangle. \quad (5)$$

However, in our implementation, this is not exactly a least-squares fit. In the usual ℓ^2 inner product definition, $\langle A, B \rangle \propto \text{mean}(A \cdot B)$, we replace the mean value with the histogram peak position, estimated with a Gaussian fit. This makes the procedure more robust with respect to magnetic signal not completely removed by the masking, as well as artifacts that often occur near the edges of the FOV.

The corrections in Eq. 4 (with weights usually on the order $\pm 10^{-3}$) are then applied to all tuning states.

4.7. Orientation and pointing

The final science data cubes are by default oriented so the pixel axis directions are along the HPLN and HPLT (solar longitude and latitude) coordinate axes. The second axis points toward solar North. The spatial coordinates can be calibrated with SDO/HMI continuum images as reference.

To calibrate the field rotation, we use data sets with some pores or spots in the FOV is needed, features for which the orientation can be recognized in the lower resolution of HMI. See Fig. 8 in the CRISPRED paper for a comparison of CRISP and HMI images of the same FOV.

The pointing information logged by the Primary Image Guider (PIG; Sliepen & Sütterlin 2013) is estimated to be correct to within $5''$ if a four-limb calibration of the PIG/Turret system was performed close in time before the data were collected but could otherwise be off by on the order of an arc minute. HMI

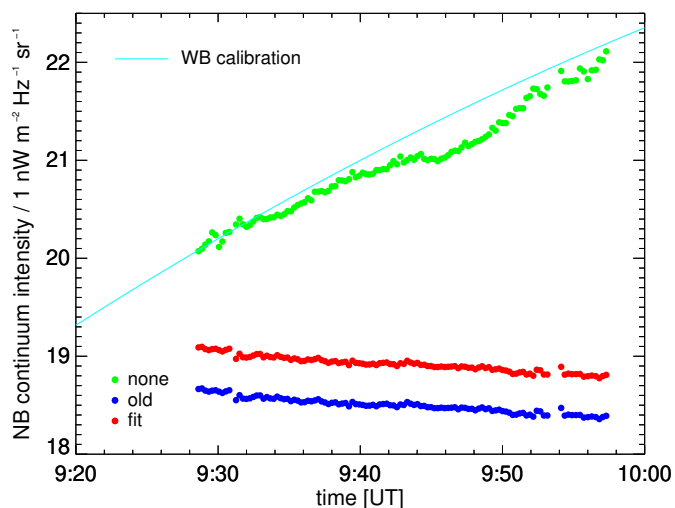


Fig. 10: CHROMIS Ca II NB continuum (median) intensities of restored data (multiple scans), with and without temporal correction as indicated in the legends. See also Fig. 9.

continuum images with spots and pores can also be used to refine the pointing metadata in the spatial WCS information.

5. Image restoration

5.1. MFBD and MOMFBD

Isoplanatic image formation with optical aberrations can be modeled as a convolution of an object with a PSF, where the PSF is determined by the variation of the wavefront phase over the pupil. The wavefront can be expanded into linear combinations of a finite set of modes that span a subspace of all possible aberrations. Multi-frame blind deconvolution (MFBD) methods, including Phase Diversity (PD, see Sect. 5.2), are based on estimating the wavefront parameters by fitting the model to a data set, where the assumption that multiple images depict the same object is a powerful constraint (see e.g., Löfdahl 2002, and references therein). With the assumption of additive white noise, the intensity of the unknown object can be calculated by deconvolution of the data so the pixel values do not have to be estimated as independent model parameters.

The wavefront aberrations are caused by turbulence in the earth’s atmosphere, randomly mixing air with different temperature and therefore different refractive index. We therefore have to make the assumption that the exposures are short enough that the PSF does not have time to change significantly. Due to turbulence at high altitudes, the line of sight from the telescope to different parts of the FOV passes through different turbulent structures, which means the image formation is not really isoplanatic. However, within sufficiently small subfields the assumption of isoplanatic image formation is a good approximation. We solve the model fitting and deconvolution problem independently within multiple subfields and form restored versions of the full FOV by mosaicking the results from the individual subfields.

For imaging spectro(polari)meters, each NB wavelength tuning and polarization state produce its own co-spatial “object”. The number of collected frames in each state is then determined by a trade-off: we need many frames to boost the SNR, particularly in the core of deep lines, but we want to complete a full scan before the solar scene evolves too much. Usually only a few

frames per state are collected, too few for MFBD to effectively restore the images independently for the individual NB states. In addition to the NB images, we also collect WB images in synchronization with the NB images, with the result that a NB line scan is always accompanied by a simultaneous WB data set that span the entire scan. The MOMFBD algorithm uses the WB and NB data together to make a joint restoration (Löfdahl 2002; van Noort et al. 2005). A CHROMIS MOMFBD dataset is illustrated in Fig. 13, CRISP is similar but without a PD channel (see Sect. 5.2). The WB *anchor* images aid the image restoration in two ways: 1) the large number of images of the same object and many realizations of the random wavefronts constrain the solution and 2) the estimated wavefront tilt components align all the WB images, and therefore also the NB images to the WB. The result is that the different NB images are aligned also to each other.

Some particular challenges related to MOMFBD image restoration with spectropolarimetric data are described by van Noort & Rouppe van der Voort (2008), Schnerr et al. (2011), and in Sect. 4.4 of the CRISPRED paper.

We use a MOMFBD code not published before (see Appendix A.3) and a few developments in how the MOMFBD processing is set up and run. The latter are described in the following subsections.

5.2. Phase diversity

The Phase Diversity (PD) wavefront sensing and image restoration technique is a form of MFBD that is constrained by the intentional defocusing of one or more images, corresponding to a known, parabolic difference in phase over the pupil⁹. The technique was invented by Gonsalves (1982) and the theory was clarified and extended to multiple diversities and multiple exposures by (Paxman et al. 1992a; Paxman et al. 1992b). It was independently developed for high-resolution solar data by Löfdahl & Scharmer (1994) and Seldin & Paxman (1994). Both implementations were verified vs. each other and vs. Speckle interferometry by Paxman et al. (1996). Löfdahl (2002) formulated it in terms of linear equality constraints (LECs), thereby incorporating it into what later became the MOMFBD method.

CHROMIS includes a WB PD camera. See Fig. 14 for a demonstration of image quality obtained with three different MOMFBD restorations of CHROMIS Ca H+K WB data: 60-mode MOMFBD with and without PD, and MOMFBD without PD and only the two tip and tilt modes corrected, corresponding to shift-and-add together with correction for the theoretical, aberration-free modulation transfer function (MTF) of the telescope. Both 60-mode restorations bring out fine structure not visible in the MTF-corrected image, but PD improves the contrast further, although it is still far from the expected Ca II continuum granulation RMS contrast in excess of 27% (Scharmer et al. 2019).

5.3. Modes

By default we use Karhunen–Loève (KL) modes to parameterize the unknown wavefronts to be estimated by the MOMFBD processing. Like Zernike polynomials, they are orthogonal on a circular pupil. In addition they are statistically independent with

⁹ The diversity in phase does not have to be focus. However, this is easily implemented and by far the most commonly used. The magnitude of the phase difference also does not have to be known, although it does constrain the solution much better if it is.

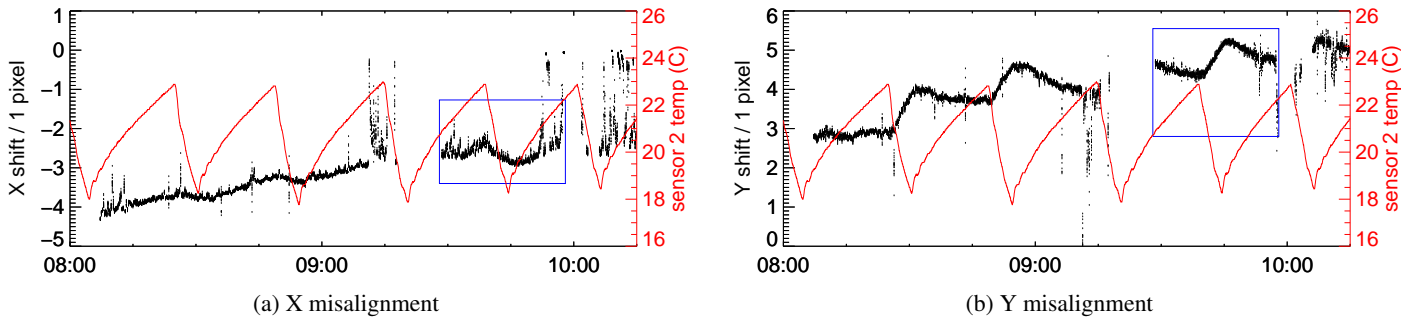


Fig. 11: Co-variation of continuum/WB misalignment measured with raw data and telescope bottom plate temperature. These data were collected during the morning hours of 2016-09-19. In bad seeing, measurements most often tend toward zero. The blue boxes correspond approximately to the plot ranges of Fig. 12(b) and (c).

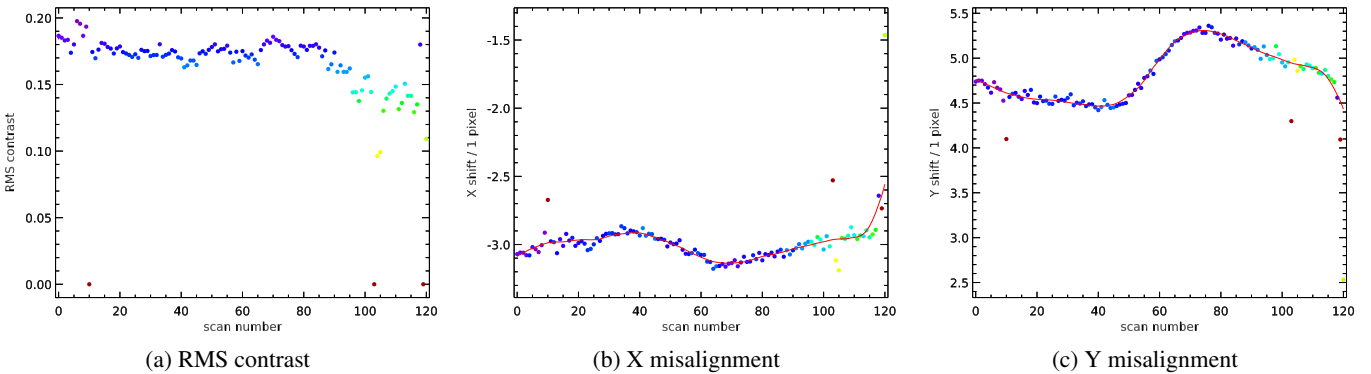


Fig. 12: Continuum alignment diagnostic plots for 121 Ca II scans collected from 09:28:36 on 2016-09-19, covering approximately one period of the undulations shown in Fig. 11. (a) WB RMS contrast; (b) Continuum/WB X misalignment; (c) Continuum/WB Y misalignment. Filled circles in (b) and (c): misalignment measured by use of cross correlation with MOMFBD restored data, colors represent RMS contrast as shown in (a). Lines in (b) and (c): shifts in X and Y used for alignment, misalignment smoothed with a heuristic algorithm that gives more weight to the high-contrast data points. Diagnostic plots like these are automatically produced by SSTRED, to allow the user to check how well the contrast-aware smoothing worked.

respect to wavefronts from atmospheric turbulence. As the SST AO monomorph deformable mirror is designed to correct such atmospheric wavefronts, the KL modes are also well suited to correcting residual wavefronts from the AO.

The KL modes implemented are based on expansion in Zernike polynomials (Roddi 1990) and therefore indexed as the dominating Zernike polynomial as ordered by Noll (1976). In this order, the expected variance from turbulent seeing does not decrease monotonically, so to make the best subset selection we have to order them first. Then we select the most significant subset by truncating the list to the wanted length.

We used to sort the selected subset of KL-modes back in index order, for no better reason than to make the list look cleaner. We have since realized that this is not optimal with respect to an important aspect of the inner workings of the MOMFBD (and REDUX) program: In order to stabilize the solution, a few iterations are run with first 5, then 10, then 15, etc., modes until all the specified modes are included. The purpose is to allow the most significant modes to determine the coarse shape of the wavefront before the finer features are fitted. This internal increase in the number of modes should therefore also be done in variance order, which means the selected set should be specified in variance order.

5.4. Residual alignment and destretching

With perfectly estimated wavefronts, the anchor WB images should force the restored images of all objects to be perfectly aligned. However, model fitting with real data is rarely perfect so there are small but noticeable residual misalignments between the NB images. There is also residual stretching (from anisoplanatic wavefront aberrations) on scales smaller than the subfields, that MOMFBD cannot compensate for.

Henriques (2012) included a technique for a post-MOMFBD dewarping step, that compensates for the residual geometrical differences between the NB images in a scan. This has since been used routinely in the CRISPRED pipeline, see Sect. 4.4.2 of the CRISPRED paper. The method is based on the MOMFBD program outputting extra deconvolved WB images, in addition to the restored anchor WB image based on all exposures in the scan. The extra WB images, one per NB state, are generated by deconvolving only the subset of the raw WB images that are simultaneous to the raw NB images of that state. The extra deconvolved WB images will be locally distorted exactly the same way as the deconvolved NB images and have the same residual misalignment. But unlike NB images from different states, these WB images can be successfully destretched against the anchor WB image to measure the local warping, which can then be applied to the NB images to get a significantly more well-aligned data cube.

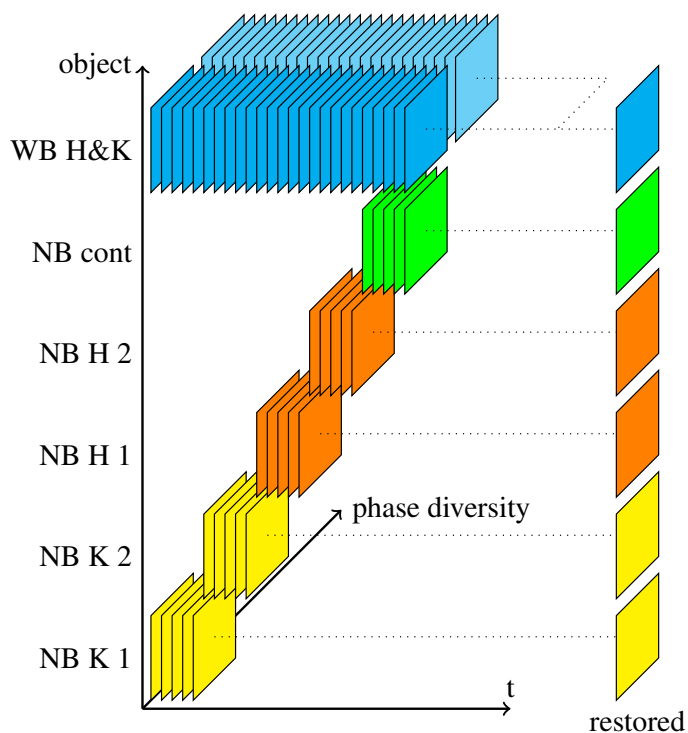


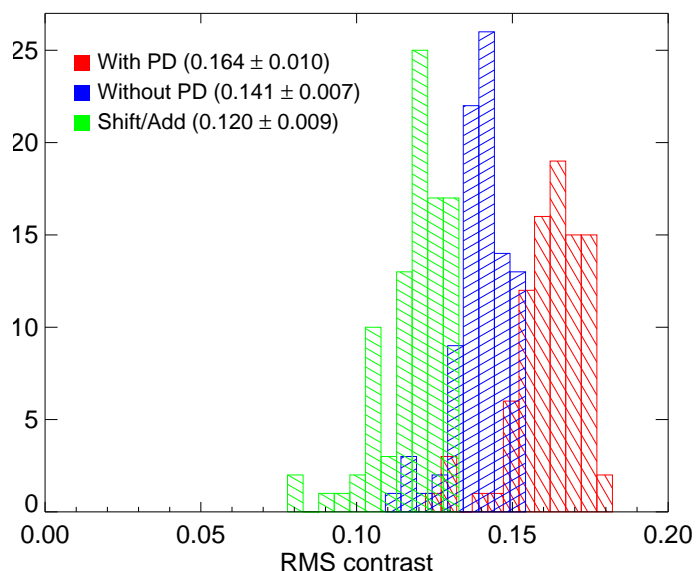
Fig. 13: Schematic representation of CHROMIS datasets for MOMFBD processing. The depicted mock dataset has a NB continuum tuning point (green), two tuning points each in a NB K filter (yellow) and a NB H filter (orange). The H&K WB filter (blue) anchors the entire scan. I.e., it forces MOMFBD to align the restored images of the scan.

We have modified the way to make the MOMFBD program generate those extra WB images. We used to specify them as them part of the MOMFBD data set, using LECs to make their estimated wavefronts identical to those of the simultaneous NB images. With zero weight in the error metric, mathematically they should not to influence the solution. However, numerically it turns out that adding these extra objects, even with zero weights, does in fact have a small, but measurable, impact on the converged solution. We attribute this to the changed LECs, and the nullspaces they generate.

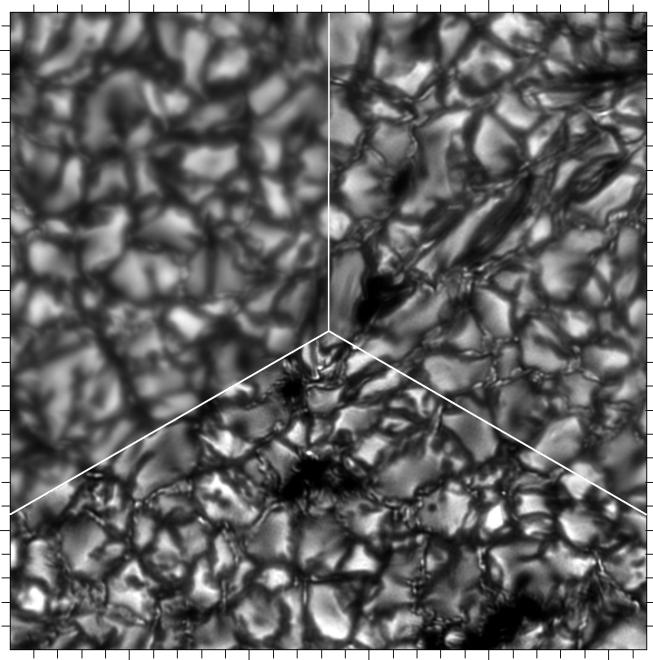
Apart from the fact that the solution is modified slightly when adding zero-weight objects to the LECs, there is another downside to the previous approach. The MOMFBD code treats the extra objects just as any other, i.e., it will load and process the WB data twice (once for the anchor object and once for the extra WB objects), which leads to a significant increase in both RAM usage and CPU load. For both CRISP and CHROMIS, the amount of data increases by 33% by this method (three co-temporal exposures are basically turned into four).

To overcome these issues, REDUX has a new mechanism, where the extra WB objects are not specified with LECs. Instead, REDUX can be configured to generate the desired images as a final step after the wavefronts have been estimated. At that point, it deconvolves subsets of the WB images, which match the frame numbers of the NB images. As no modifications are made to the problem itself, this will not interfere with the solution at all.

In practice, although the converged solutions differ, the quality of the restored data is similar. The real advantage of not including the extra WB objects in the problem with LECs is that fewer gradients of the error metric need to be calculated. For



(a) RMS contrast histograms. The numbers in parentheses are the median \pm the (robust) standard deviations of the contrasts.



(b) One example of the FOV used in ((a)), comparing the three different levels of processing. The tickmarks are 1'' apart. Top left: shift-and-add and MTF correction; top right: 60 modes MFBD; bottom: 60 modes MFBD with PD.

Fig. 14: Contrast and image quality after different levels of MOMFBD restoration of CHROMIS Ca II continuum images from 110 scans collected on 2016-09-19. The FOV is 700 \times 700 pixels (26''5 \times 26''5). Processing levels: MFBD with and without PD using 60 KL modes, without PD using only tilt modes (corresponding to shift-and-add by subfield and MTF correction).

a typical CRISP or CHROMIS data set with three cameras this means a \sim 25% reduction in the processing time.

6. Metadata

For metadata, we follow the SOLARNET recommendations of Haugan & Fredvik (2020). The idea is that data should have enough metadata that “a Solar Virtual Observatory (SVO) be able to [...] find sets of successful observations matching a hypothetical ideal observation proposal (if such observations exist).” The SOLARNET recommendations are an attempt to standardize metadata between multiple telescopes and instruments so that searches can be “instrument agnostic”. The metadata should also facilitate correct interpretation of data by a researcher who was not involved in the observations, nor the pipeline processing. That is, they should be complete enough that all important circumstances of the observations are included. Also the processing done by the pipeline should be documented in the metadata, in particular when a processing step could be run with different parameter settings.

We store science-ready data in FITS format (Pence et al. 2010) with metadata information in the form of FITS header keywords and extensions.

Some information is difficult to fit in standard FITS header keywords. A number of conventions have therefore been developed, for making it easier to store particular kinds of information in FITS files. We use

- the record-valued keywords of Calabretta et al. (2004) for representing coordinate distortions.
- the JavaScript Object Notation (JSON; Bray 2014) for encoding FITS keywords with structured contents as strings, such as the SOLARNET PRPARAn keywords. JSON was developed for JavaScript but is now implemented in all major programming languages.
- the SOLARNET *variable keywords* (Haugan & Fredvik 2015; 2020), a mechanism for associating auxiliary data with the main data in a FITS file,¹⁰ for intensity statistics and some metadata from the log files of auxiliary instruments.

6.1. SOLARNET compliance and support

A FITS file can be SOLARNET compliant partially or fully. For partial compliance, it is enough to include a small number of (four) mandatory header keywords and, if there are keywords that are used in conflict with the definitions in the SOLARNET recommendations, a fifth keyword with a list of such keywords. For full compliance, a larger set of mandatory keywords must be used *depending on the nature of the observation*. The level of SOLARNET compliance is itself indicated with the mandatory header keyword SOLARNET, values 0.5 for partial compliance and 1 for full compliance.

SSTRED’s SOLARNET-compliant science data cubes are supported by the CRISP SPectral EXplorer (CRISPEX; Vissers & Rouppe van der Voort 2012), version 1.7.4 (released in January 2018) or later, see also Sect. 7. SOLARNET compliance should make it easier for future data viewing and analysis programs to support data from multiple sources.

In addition to SSTRED, several data pipelines are or will be preparing their metadata in compliance with the SOLARNET recommendations. The sTools pipeline is partially SOLARNET-compliant (Denker et al. 2018). The pipeline of SPICE produces

¹⁰ The SOLARNET variable keywords are stored in FITS binary-table extensions and are associated with single-value regular header keywords. What to use for the regular header keyword value is not defined, but it is supposed to represent the whole cube in a way that makes sense for the particular quantity.

SOLARNET-compliant output. The Astronomical Institute of the Slovak Academy of Sciences (AISAS) is updating their data pipelines, developed for the Coronal Multi-channel Polarimeter for Slovakia (CoMP-S; Kučera et al. 2010) and the Solar Chromospheric Detector (SCD; Kučera et al. 2015) instruments of the Lomnický Štít Observatory, according to the SOLARNET Metadata Recommendations (J. Rybák and P. Gömöry 2020, priv. comm.). The recently funded Solar Activity Monitor NETWORK (SAMNET) project are planning to follow the SOLARNET recommendations for their data structure (R. Erdélyi 2020, priv. comm.). The Royal Observatory of Belgium (ROB) are aiming at producing, from early 2021, image datasets from the Uccle Solar Equatorial Table (USET; Berghmans et al. 2005) in white light, $H\alpha$, and Ca II K with SOLARNET compliant headers (R. Vansintjan 2020, priv. comm.). The Solar ALMA Pipeline (SoAP; Szydlarski 2019) will follow the SOLARNET recommendations (Haugan & Fredvik 2020).

This is evidence that the SOLARNET metadata recommendations have gained momentum and do provide a means of metadata standardization that should significantly aid the analysis of data, in particular co-analysis of data from multiple instruments and telescopes.

6.2. Observations

Passing metadata from the observations through the SSTRED processing, including the many calibration steps, requires access to metadata pertaining to the details of the observations. This metadata has to be collected from multiple sources, such as log files from auxiliary instruments as well as the raw image data files themselves.

6.2.1. Image data

The metadata collected from the raw data files include prefilter, tuning and polarimetry states, the detector used, time stamps, exposure times, etc.

CHROMIS raw data are stored in multi-frame FITS files with metadata in the headers while CRISP raw data are stored one frame per file in ANA’s fz format. The latter format has less structured headers and a lot of the metadata is therefore encoded in the file names.

The reading of metadata from the raw files in a structured way turned out to be a major bottleneck in SSTRED processing. Particularly for CRISP, where each frame has a file header to be read and a file name to be parsed. We therefore started experimenting with ways of speeding this up.

A first attempt was to implement a Dynamically Loadable Module (DLM) that could be used to cache this information, so SSTRED at least didn’t have to read the same information more than once in the same IDL session. This was mainly useful for development and testing but did not really help regular users, who generally only process the same data once.

Recently, we implemented code that reads all the raw-file metadata already at the time of the observations, and writes it in a database. For users with access to the database, this makes a very significant speedup in SSTRED processing that depends on the file system and the current load. A few tests with reading metadata for 50,000 CRISP frames (corresponding to 7.5 min of observations) took 20–45 min from the files and 25–40 s from the database. So for large data sets we have a reduction from hours to minutes by reading metadata from the database.

When accessing metadata for older data, not already in the database, during normal operations, SSTRED automatically falls back to reading the metadata from the data files and then adds them to the database (effectively serving as a cache that is persistent between IDL sessions).

The database is running on a MariaDB server. To avoid redundancy, it is organized in hierarchical, linked tables with columns of metadata appropriate for each level, see Table 3. In addition, there are auxiliary tables with information about image detectors and prefilters.

The tables have *unique* constraints to prevent writing the same information in multiple rows. They also have *foreign key* constraints that prevent deletion of information from connected rows in different tables.

As of this writing, the database is available only for users at the Institute for Solar Physics in Stockholm but we plan to make it more widely available after a testing period.

6.2.2. Auxiliary instruments

We extract some metadata from auxiliary instruments for the available points in time within the span of the science data in a data cube. These metadata are stored as SOLARNET variable keywords.

From the Turret log file, we read the elevation angle.

The AO log file provides the AO lock rate as well as two estimates of the Fried parameter r_0 . One of the r_0 values measures mostly ground layer seeing while the other includes also high-altitude seeing (Scharmer et al. 2019).

6.3. World Coordinate System

Following the SOLARNET recommendations, we use the World Coordinate System (WCS) to describe the observations. The WCS is part of the FITS standard 3.0 (Pence et al. 2010, their Sect. 8) and it allows the specification of coordinates for all (multi-dimensional) pixels of a data cube. More details can be found in a series of papers started by Greisen & Calabretta (2002) and continued by authors cited in the subsections below.

For our five-dimensional science-ready data cubes, the relevant coordinates are spatial, temporal, spectral, and polarimetric. The WCS part of a sample FITS header produced by SSTRED is shown in Fig. 15. As specified with the `PSI_0` keywords, all our coordinates (except Stokes) are tabulated in a FITS extension named `WCS-TAB`, in columns numbered as given by the `PVi_3` keywords.

6.3.1. Spatial coordinates

The WCS for *spatial* coordinates was defined by Calabretta & Greisen (2002). (Thompson 2006; 2010b) extended the notation with coordinates relevant to Solar observations.

Our spatial coordinates are obtained from PIG. PIG fits a circle to the circumference of the primary image of the solar disk, as projected on the bottom plate of the telescope vacuum tube. Knowing the location of the exit window, it infers the pointing with $\sim 10''$ accuracy and $\sim 1''$ precision and logs it every second¹¹. However, the accuracy depends on a recent calibration, with several positions on the limb as reference. Failing that, the pointing can be $1-2'$ off.

¹¹ It is rare, but PIG sometimes loses track of the Solar disk for extended periods of time. When it does, SSTRED falls back to the less accurate spatial coordinates from the Turret, logged every 30 s.

SSTRED interpolates the logged coordinates to get the pointing for any point in time.

All frames that belong to the same scan are aligned by the MOMFBD processing so that they all have a common FOV. The temporal alignment procedure follows the features in the photospheric WB images, trying to keep them stationary in the FOV. This means the spatial coordinates are constant during a scan but can change with scan number due to the Solar rotation and possibly the motion of the tracked feature over the solar surface. However, with the expected limited accuracy of the pointing information initially we set the spatial coordinates to the median of the logged pointing coordinates. Varying coordinates can be introduced later with calibrations to other instruments.

We specify the spatial coordinates by tabulating them for the array corner pixels for each scan, a capable WCS reader can then interpolate to get the coordinates for any pixel.

Before May 2020, SSTRED did not have an absolute calibration of the orientation of the cameras with respect to the solar coordinate system. It can now do this (also for older data) by fitting SST images of a suitable target to simultaneous SDO/HMI continuum images. Before, only the average of the four corner coordinates could be trusted as the coordinates of the center of the FOV. The lack of orientation information is signaled by setting the systematic accuracy (keyword `CSYERn`) for the spatial coordinates to $60''$ or worse (comparable to the entire FOV). When the calibration is done, `CSYERn` is set to $5''$ or less.

6.3.2. Spectral coordinates

The *spectral* coordinates (Greisen et al. 2006) are initially set by the tuning sequence decided by the observer. Because they are in general not equidistant, they have to be tabulated.

Small adjustments of the wavelength scale are made based on a calibration of disk center data vs. an atlas spectrum (see Sect. 4.4.1). The cavity errors (see Sect. 4.2) are stored as distortions to the wavelength coordinate by use of notation that extends the WCS formalism, see Appendix B.

Before we implemented correction of the wavelengths based on the spectral calibration (Sect. 4.4.1), the wavelength of the line core had to be calibrated for each target individually and it depends on the position of the observed target on the solar disk. For example, de la Cruz Rodríguez et al. (2011) provides a calibration method based on synthetic spectra derived from 3D MHD simulations of the solar photosphere, and later studies by Löhner-Böttcher et al. (2017) and Löhner-Böttcher et al. (2018) propose to calibrate observations using laser based measurements.

Recent atmospheric model inversion codes like NICOLE (Socas-Navarro et al. 2015) and STiC (de la Cruz Rodríguez et al. 2016) need information about pixel and line dependent wavelength shifts originating from, e.g., cavity errors. When the observations all have the same cavity errors, a correction can be applied afterwards, to the estimated velocities. But for multi-line and multi-instrument data, the inversions need instrumental profiles customized for each spectral region and pixel.

6.3.3. Polarimetric coordinates

In the WCS, the *polarimetric* coordinates for Stokes vectors are defined as indices [1, 2, 3, 4] for the $[I, Q, U, V]$ components (Greisen & Calabretta 2002). The Stokes Q , U , and V components are defined with respect to a frame of reference, such as a Cartesian coordinate system with axes (x, y, z) , where $Q > 0$

Table 3: Metadata database tables

Name	Range	Types of metadata
datasets	Data sets	Date and time of a data-set start, type, ^a instrument name
configs	Group of files	Camera name, ^b gain, exposure time, frame dimensions, number of frames per file, average cadence etc.
bursts	Burst of exposures ^c	Date and time of beginning of burst, prefilter, FPI tuning, scan number, frame number of first frame, detector temperature.
chromis_frames	Individual frames	Time, frame number, intensity statistics.
crisp_frames	Individual frames	Like <code>chromis_frames</code> + liquid crystal state
crisp_polcal_frames	Individual frames	Like <code>crisp_frames</code> + quarter-wave plate angle, linear polarizer angle.

Notes. Hierarchical tables, parents on top.

^(a) Types of data sets are darks, flats, science, etc. ^(b) The camera name here is the functional name of a camera, like Crisp-R (CRISP NB camera in the beam reflected by polarizing beamsplitter), Chromis-W (CHROMIS WB camera), etc. ^(c) By burst we refer to a group of image frames with identical tuning and polarization states, collected during a short period of time, to be processed with the assumption that the Sun does not change. For CHROMIS a single file, for CRISP a group of files.

($Q < 0$) denotes linear polarization along the x (y) axis, $U > 0$ ($U < 0$) denotes linear polarization along the line $y = x$ ($y = -x$), and $V > 0$ ($V < 0$) denotes right-handed (left-handed) circular polarization around the z axis.

Our reference system is oriented so x is parallel to the HPLT axis (Solar North) and y is antiparallel to the HPLN axis, which form a right-handed system together with a z axis pointing along the propagation axis. However, the WCS surprisingly does not seem to have a general notation for describing the orientation of the Stokes reference system.

There are two Stokes reference system conventions in use in the night-time community, both based on the equatorial coordinate system (Right Ascension and Declination) but with the third axis pointing in different directions (toward or away from the observer, respectively). To break the ambiguity, Górski et al. (2010) defined the FITS header keyword POLCCONV for the Hierarchical Equal Area iso-Latitude Pixelization (HEALPix) data structure, used for sky maps from various sources. Their POLCCONV has two possible string values, 'IAU' and 'COSMO' for those two conventions.

Equatorial coordinates are not practical for high-resolution Solar observations, where we are more interested in coordinates on the solar disk than the Sun's position on the sky. The latest version of the SOLARNET recommendations (Haugan & Fredvik 2020) recommends a right-handed coordinate system with the z axis oriented towards the observer as for the IAU convention (Heeschen et al. 1973). The axes are specified with an extended use of POLCCONV in the form '(±XXXX, ±YYYY, ±ZZZZ)', where XXXX, YYYY, and ZZZZ are names of WCS coordinates and a plus (minus) means the axis is parallel (antiparallel) to the named coordinate.

Thus, we specify our reference system with POLCCONV = '(+HPLT, -HPLN, +HPRZ)',¹² where HPRZ is defined as the axis pointing toward the observer (Thompson 2006).

This use of POLCCONV could serve as a general notation. For example, the right-handed equatorial IAU system mentioned above can be specified as POLCCONV = '(+RA--, +DEC-, -DIST)', where DIST, defined as the "radial distance from the observer", points away from the observer. The left-handed COSMO system is then POLCCONV = '(+RA--, +DEC-, +DIST)'.

¹² When developing notation for the POLCCONV keyword, we initially specified only the first two axes. So for SST data, when the third axis is omitted, +HPRZ is implied.

6.3.4. Temporal coordinates

Temporal WCS coordinates are described by Rots et al. (2015).

Due to varying delays from FPI tuning and prefilter changes during spectral scans, the *temporal* coordinates in our data cubes are not equidistant and therefore have to be tabulated. Time is read from the metadata of each raw-data frame and averaged for the frames that were combined (by MOMFBD restoration) to make a frame in the data cube.

Time is advanced not only from one scan to the next, but also from one tuning position to the next. Polarimetric states are varied multiple times per tuning state so the restored images are made from data with overlapping time. These images are then mixed in approximately equal proportions by demodulation into Stokes components. Because of this we assign the same time coordinate to all Stokes components of the same tuning state.

6.3.5. Telescope location

The telescope location is specified in three dimensions with the keywords OBSGEO-X, OBSGEO-Y, OBSGEO-Z (Rots et al. 2015, their Sect. 4.1.3). We have calculated the values of those keywords (as shown in Fig. 15) following their recipe. As input we used the geodetic location of the SST, (latitude, longitude, altitude) = (28°759693, -17°880757, 2380 m).

These numbers come from two services provided by Google. The latitude and longitude is available with high precision by selection of a location in google maps.¹³ They also run a separate elevation service,¹⁴ by use of which the altitude of the SST location was determined to a few meters above 2360 m. Allowing for the SST tower, the adopted altitude value is 2380 m.

The accuracy is estimated to ~10 m, which should be sufficient for calculations of relative speeds vs the Sun.

6.4. Statistics

The SOLARNET recommendations include the statistics metadata keywords in Table 4. One purpose of this is to make it possible to include intensity statistics in data archive search criteria.

In addition to the keywords in Table 4, there is a DATARMS keyword in the SOLARNET recommendations. However, as

¹³ <https://goo.gl/maps/XwGtEU6ueZv>

¹⁴ <https://developers.google.com/maps/documentation/javascript/examples/elevation-simple>

```

PC1_1 = 1.00000 / No rotations
PC2_2 = 1.00000 / No rotations
PC3_3 = 1.00000 / No rotations
PC4_4 = 1.00000 / No rotations
PC5_5 = 1.00000 / No rotations

CTYPE1 = 'HPLN-TAB' / SOLAR X
CUNIT1 = 'arcsec' / Unit along axis 1
CNAME1 = 'Spatial X' /
PS1_0 = 'WCS-TAB' / EXTNAME; EXTVER=EXTLEVEL=1 is default
PS1_1 = 'HPLN+HPLT+WAVE+TIME' / TTYPE for column w/coordinates
PS1_2 = 'HPLN-INDEX' / TTYPE for INDEX
PV1_3 = 1 / Coord. 1 tabulated coordinate number
CRPIX1 = 0 / Unity transform
CRVAL1 = 0 / Unity transform
CDELTA1 = 1 / Unity transform
CSYER1 = 60 / Orientation unknown

CTYPE2 = 'HPLT-TAB' / SOLAR Y
CUNIT2 = 'arcsec' / Unit along axis 2
CNAME2 = 'Spatial Y' /
PS2_0 = 'WCS-TAB' / EXTNAME; EXTVER=EXTLEVEL=1 is default
PS2_1 = 'HPLN+HPLT+WAVE+TIME' / TTYPE for column w/coordinates
PS2_2 = 'HPLT-INDEX' / TTYPE for INDEX
PV2_3 = 2 / Coord. 2 tabulated coordinate number
CRPIX2 = 0 / Unity transform
CRVAL2 = 0 / Unity transform
CDELTA2 = 1 / Unity transform
CSYER2 = 60 / Orientation unknown

CTYPE3 = 'WAVE-TAB' / Wavelength, function of tuning and scan number
CNAME3 = 'Wavelength' /
CUNIT3 = 'nm' / Wavelength unit, tabulated for dim. 3 and 5
PS3_0 = 'WCS-TAB' / EXTNAME; EXTVER=EXTLEVEL=1 is default
PS3_1 = 'HPLN+HPLT+WAVE+TIME' / TTYPE for column w/coordinates
PV3_3 = 3 / Coord. 3 tabulated coordinate number
CRPIX3 = 0 / Unity transform
CRVAL3 = 0 / Unity transform
CDELTA3 = 1 / Unity transform

CTYPE4 = 'STOKES' / Stokes vector [I,Q,U,V]
CRPIX4 = 1 / First (and only) quantity is I
CRVAL4 = 1 / First (and only) quantity is I
CDELTA4 = 1 / [1,2,3,4] = [I,Q,U,V]

CTYPE5 = 'UTC--TAB' / Time, function of tuning and scan number
CNAME5 = 'Time since DATEREF, increases with dim. 3 and 5' /
CUNIT5 = 's' /
PS5_0 = 'WCS-TAB' / EXTNAME; EXTVER=EXTLEVEL=1 is default
PS5_1 = 'HPLN+HPLT+WAVE+TIME' / TTYPE for column w/coordinates
PV5_3 = 4 / Coord. 5 tabulated coordinate number
CRPIX5 = 0 / Unity transform
CRVAL5 = 0 / Unity transform
CDELTA5 = 1 / Unity transform

TIMESYS = 'UTC' /
DATEREF = '2016-09-19T00:00:00.000000' / Reference time in ISO-8601
OBSGEO-X= 5327386 / [m] SST location
OBSGEO-Y= -1718721 / [m] SST location
OBSGEO-Z= 3051720 / [m] SST location

```

Fig. 15: WCS part of sample FITS header without polarimetry.

DATANRMS is just DATARMS normalized with DATAMEAN, including all three quantities would be redundant. We believe DATANRMS, corresponding to what is commonly known as the RMS contrast, is the more useful quantity for making quality-based searches in an SVO.

These statistical keywords are stored as SOLARNET variable keywords, one value per frame in science data cubes. These values are easy to calculate as the cube is written to file, frame by frame.

Table 4: Statistics metadata keywords

Keyword	Description
DATAMIN	The minimum data value.
DATAMAX	The maximum data value.
DATAP nn	the nn percentile, where $nn \in \{01, 02, 05, 10, 25, 75, 90, 95, 98, 99\}$.
DATAMEDN	The median data value \equiv the 50 percentile.
DATAMEAN	The average data value.
DATANRMS	The normalized RMS deviation from the mean.
DATASKEW	The skewness.
DATAKURT	The excess kurtosis.
DATAMAD	The mean absolute deviation from the mean.
NDATAPIX	The number of data pixels, excluding padding and other missing-data pixels.

Notes. We use a subset of the statistics metadata keywords from the SOLARNET recommendations.

We also need regular header keyword values that go with these variable keywords, that represent statistics for the whole cube. The minimum and maximum values for the whole cube are easy to calculate, they are just the minimum and maximum, resp., of the per-frame minimum and maximum values. Moments and percentiles require special attention because their calculation with built-in IDL commands requires that the whole cubes are in memory. The NB cubes are potentially too large for this (this is the reason CRISPEX needs the two, differently ordered versions of the cubes for fast access, see Sect. C.2). So we need alternate ways to compute them.

Pébay et al. (2016) give numerically stable one-pass expressions for the mean, $\bar{x} = \frac{1}{n} \sum_{i=1}^n x_i$, as well as the central moments, $\mu_p = \frac{1}{n} \sum_{i=1}^n (x_i - \bar{x})^p$ for any $p \geq 2$, from which RMS, skewness, and kurtosis can be calculated. However, we want to calculate the quantities for the whole cube from those of the individual frames so instead we use their “pairwise” formulas to combine the per-frame quantities as described in Appendix D.

The cube percentiles cannot be calculated from the per-frame percentiles. Instead, we calculate (approximate) percentile values (including the median) from a cumulative histogram for the entire cube, accumulated frame by frame, using a large number of bins (now $2^{16} = 65536$ bins). The percentile values can then be found as the data values corresponding to the first bins that exceed the percentiles. The accuracy of percentiles calculated in this way should be on the order of the bin size (i.e., the range of values in the cube divided by the number of bins). Assuming the data values are evenly distributed within the bins, we further improve the accuracy by at least an order of magnitude by use of interpolation.

The mean absolute deviation from the mean (MAD) was a late addition to the included statistics. Like the percentiles, it can not be calculated for the whole cube from the per-frame values. This value is instead built up during the histogram accumulation pass through the cube, the mean being known from the first pass.¹⁵

¹⁵ The fact that we make two passes removes one advantage with the pair-wise expressions in Appendix D, as we could then use the two passes also for the moments. If computing time is of the essence, one could consider using a simple mean of the per-frame values for the regular header keyword.

7. CRISPEX

An important part of the workflow with complex data products like the science-ready data cubes produced by SSTRED is being able to view and analyse them. Not a part of SSTRED per se, the CRISP SPECTRAL EXPLORER¹⁶ (CRISPEX; Vissers & Roupe van der Voort 2012) is an IDL tool that offers such data cube browsing and analysis functionality.

From version 1.7.4, released in January 2018, CRISPEX supports the SOLARNET compliant science data cubes output by SSTRED.

CRISPEX was originally developed for CRISP science data cubes stored in LP format files.¹⁷ CRISPEX was earlier extended to support data from the Interface Region Imaging Spectrograph (IRIS; De Pontieu et al. 2014), reading both its Level 3 spectrograph (SG) FITS cube files and the Level 2 slit-jaw image (SJI) files¹⁸. In fact, CRISPEX can handle any synthetic or observational data cube, provided it has been formatted according to either the legacy LP format, the SOLARNET compliant FITS format, or the IRIS FITS format (e.g., IRIS SJI-formatted SDO and Hinode data, or IRIS SG-formatted Bifrost cubes).

The richer metadata in the SOLARNET cubes should result in an improved user experience compared to the LP format cubes (and to some extent also compared to the IRIS format), both when calling the program and during run-time. During run-time the changes are visible mostly when dealing with the WCS information, see Sect. 6.3. For instance, while the LP and IRIS formats provide only scan-averaged time, the SOLARNET format’s WCS information contains image timing information as function of wavelength tuning and modulation state (for tuning instruments) or of spatial position and modulation state (for (scanning) slit spectrographs). Also, the time-dependent spatial position is available, which allows accounting for Solar rotation during the observations when returning the Solar spatial coordinates. This is particularly beneficial for browsing multi-instrument data sets (e.g., CRISP plus CHROMIS, CRISP/CHROMIS plus IRIS, etc.). Firstly, because the image to be displayed (determined through nearest-neighbour interpolation in time) can be selected more closely in time when considering tuning filter instruments or (rastering) spectrographs. Secondly, because one could in principle skip creating co-aligned cubes, assuming the (time-dependent) spatial coordinates are well-defined: the pixel size difference, xy -translation, FOV rotation with respect to solar north and solar rotation would automatically be taken into account during run-time through the WCS information of the respective files.

Worth noting is also that to accommodate the larger size CHROMIS images (compared to CRISP and IRIS), the zooming functionality has been extended to allow zoom true to size (i.e., 1:1 data-vs-monitor pixel scale) also on screens that would normally not fit the image. This could in the future also be useful for visualising data from the Daniel K. Inouye Solar Telescope (DKIST) or the European Solar Telescope (EST) that are set to deliver 4k×4k images.

The metadata needed, particularly the coordinate system of the data, is provided in different ways for the different file for-

¹⁶ Details such as the changelog, how to keep an up-to-date distribution of CRISPEX, and a short usage tutorial can be found on the CRISPEX github page: <https://github.com/grviss/crispex>.

¹⁷ Along with the fz format, the LP (for “La Palma”) format has been used for SST/SVST data since at least the early nineties.

¹⁸ See also the IRIS Technical Notes (ITN) 11 and 12 – concerning data levels and header keywords, respectively – on the IRIS website: <https://iris.lmsal.com/documents.html>.

mats. For smooth display and for plotting of large data cubes, the data itself needs to be ordered optimally for fast access. Details are given in Appendix C.

8. Discussion

8.1. Processing

SSTRED is a data processing pipeline that processes raw data from CRISP and CHROMIS and outputs science data cubes in FITS files.

We identified two deficiencies with CHROMIS data that we had not encountered in CRISP data. Wavelength- and time-dependent dispersion in both atmosphere and optics caused misalignment within Ca II scans. An alignment procedure was implemented as part of SSTRED. Wavelength dependent dispersion appears to limit also the accuracy of the intensity calibration, measured in the WB but applied to all wavelengths. The cause for these two issues is the wide wavelength range in Ca II scans compared to other line scans collected with CRISP and CHROMIS, together with the large wavelength gradient of the dispersion in the 400 nm region.

Making science cubes from MOMFBD-restored images involves multiple spatial corrections, such as alignment, rotation, temporal destretching to remove anisoplanatic distortions, and inter-tuning destretching to remove MOMFBD-residual geometrical distortions. Some of these operations require one correction to be applied before another is measured, causing multiple, consecutive interpolation operations. As each interpolation is a blurring operation, we want to minimize the number of such operations. Instead of performing these resampling operations consecutively, SSTRED can combine measured image shifts, rotations, and spatial distortions into a single interpolation operation, resulting in less blurring and fewer artifacts. Future pipeline developers, designing code from scratch, should build such capabilities in at a low level, perhaps by making images class objects. The objects could include both original image data, a version with operations so far performed on them, as well as a record of those operations. This way, when further operations are added, a new version can be calculated using the original data and the combined operations.

Limb data is not as well supported as on-disk data. This has to do with difficulties with alignment. The alignment between WB and NB outside the limb suffers from weak signals in the WB and continuum. On disk, there can be problems with low contrast of features on the disk and also with finding a rectangular subfield on the disk to do cross correlation on.

8.2. Metadata

SSTRED processes metadata and the output science data cubes are compliant with the SOLARNET metadata recommendations as formulated by Haugan & Fredvik (2020). This is meant to facilitate interpretations as well as the searching for science data in future Solar Virtual Observatories (SVOs). As part of SOLARNET compliance, we specify the coordinates of the output data cubes within the WCS system.

The number of pipelines that produce SOLARNET-compliant output is growing. Any new instrument and pipeline should implement this from the start. The metadata and SVO upload will facilitate the Findability, Accessibility, Interoperability, and Reusability (FAIR; Wilkinson et al. 2016) of the data.

Metadata processing posed a few new challenges to the pipeline development, leading to new developments. The time-

consuming reading of header data led to the implementation of a database for raw-data metadata. Cavity errors, pixel-dependent deviations from the nominal wavelength coordinate, required an extension of an already proposed notation for WCS coordinate distortions. While not (yet) part of WCS proper, adoption of this notation by other pipelines would simplify the task of writing software for the analysis of data from multiple instruments. By storing intensity statistics in the metadata, frame by frame as variable keywords, we can calculate some of the statistics (the moments) of data cubes from the statistics of the individual frames. An SVO that implements this capability can facilitate searches by quickly calculating statistics of subsets of data cubes from those of the individual frames.

8.3. Development

SSTRED was first developed for CHROMIS data, generalizing the old CRISPRED pipeline and adding metadata support. It should be fairly easy to extend it to process data from other, similar instruments.

The development was done by a very small team, after CHROMIS was installed. The development of the IDL parts of SSTRED has occupied one of us (MGL) for a large fraction of his time since the installation of CHROMIS. Another (TH) spent considerable time on REDUX. Together with the time spent by the remaining authors, and counting also the development of CRISPRED prior to the CHROMIS installation, this represents an effort of several person-years. This is costly, but an effort that is clearly needed to maximize the scientific output of modern ground-based solar instrumentation.

Development of new calibrations has led to new recommendations for SST observations, e.g., collecting small data sets of disk center, quiet Sun data every now and then throughout the observing period to facilitate the intensity calibration. Artifacts are to be expected and it is important to identify and characterize them as soon as possible and if possible develop procedures for compensating for them.

The SOLARNET recommendations include versioning of data files. We take that to include also intermediate data files, like calibration data that can perhaps be fitted in various ways or are based on parameters that depend on the specific use case of the data. To make the final data completely specified, versions of such data files need to be specified in the metadata. This is rather complicated and probably needs to be implemented at the core level of the pipeline. We have chosen not to do this but next-generation pipelines should be designed with this in mind.

We rely on a few external IDL libraries, that are self-contained and available through git version control (IDLastro and Coyote) or direct download from a web site (mpfit). We made an early decision not to require users to install SolarSoft (Freeland & Handy 1998) to run SSTRED. While this prevented us from using the WCS routines of Thompson (2010a) within the pipeline, we still wanted SolarSoft users to be able to use its WCS support when reading SSTRED output. Testing showed that while our five-dimensional data cubes complied with the WCS definitions, SolarSoft could not perform the required interpolation in more than three coordinate dimensions with routines included in IDL. We found the multi-dimensional interpolation implementation of Smith (2003), which is now included in Solarsoft.

SST granulation images can be aligned to HMI images with very good precision as demonstrated by R. Rutten (2020, priv. comm.) but that requires HMI data with high enough cadence that one can find a frame close enough in time that the gran-

ulation pattern has not changed too much. Not using SolarSoft within SSTRED limited also our use of HMI data to 15-min cadence publicly jpeg images available through predictable URLs. We did not find a way to programmatically download HMI 45-s cadence science data without Solarsoft. This is the reason our pointing calibration vs. HMI data so far only works for data with spots or pores in the FOV.

8.4. Data access

Access to science-ready CRISP and CHROMIS data depends on the data policies of the owners of the data. Data that belong to the Institute for Solar Physics are presently proprietary but are shared with researchers based in Sweden. Data collected within the SOLARNET access programme is proprietary for one year after successful pipeline processing and then released to the solar community. Access to data collected by other research groups depends on their data policies.

The SVO (see Sect. 3.4) database has access information and can serve download URLs. Our own data, as well as data collected under the second SOLARNET project's access programme are hosted by Stockholm University from where they can be downloaded, depending on the release status. The data download is straight forward for data that are released to the solar community, but download of proprietary data is password protected.

The Institute of Theoretical Astrophysics in Oslo and LM-SAL have released co-aligned SST/IRIS data sets elsewhere (Roupe van der Voort et al. 2020).

8.5. Concluding remarks

In this paper we describe the SSTRED data processing pipeline. We also try to demonstrate what needs to go into the pipelines of a major ground-based solar telescope and its instruments.

A pipeline that encodes optimized processing of data and calibrations is absolutely necessary for a non-trivial instrument to reach its full scientific potential. Known sources of error need to be at least characterized and when possible compensated for.

Well defined metadata are crucial for data to be usable for scientists with little knowledge about the instruments and the circumstances of the observations. We aim to follow and establish mechanisms and notation to fully characterize the output from the pipeline.

The development of SSTRED was done while the instruments and the pipeline were used, which means that early versions of the pipeline were less capable than the current one. For future telescopes, we must improve on this by having full support very soon after commissioning and also very well controlled data collection procedures. A pipeline can only work with the data that were collected and the quality of the processed data strongly depends on the calibration data collected. We cannot and should not stop development of better processing procedures, so we should collect more calibration and environment data than we know we need. As an example, having a log of the temperature sensor data from the telescope bottom plate made it much easier to understand the wavelength- and time-dependent misalignment of Ca II CHROMIS data.

All software must be expected to have bugs. Therefore, it is extremely important to archive not only reduced data but also raw data, including calibration data, at least for observations that are of lasting value and/or are difficult to repeat (unusual events, part of long time sequences, etc.). While developing SSTRED,

we have often found reasons to reprocess data, sometimes multiple times, because of corrected bugs or the addition of improved procedures. Retaining that possibility is one way of ensuring the best quality data for scientific interpretation.

We believe that SSTRED represents the most ambitious data processing pipeline for solar imaging instruments and thus can serve as a reference for future similar developments.

Acknowledgements. Guus Sliepen implemented the new data acquisition system used for CHROMIS. We have had valuable discussions about metadata and FITS headers with Mats Carlsson and Bill Thompson. We are grateful to several users – in particular Vasco Henriques and Pradeep Chitta – for patiently testing SSTRED and reporting bugs. Lewis Fox helped with the coding in the early stages of development. This work was carried out as a part of the SOLARNET project supported by the European Commission's 7th Framework Programme under grant agreement No. 312495. This research has received financial support from the European Union's Horizon 2020 research and innovation program under grant agreement No. 824135 (SOLARNET). The Swedish 1-m Solar Telescope is operated on the island of La Palma by the Institute for Solar Physics in the Spanish Observatorio del Roque de los Muchachos of the Instituto de Astrofísica de Canarias. The Institute for Solar Physics is supported by a grant for research infrastructures of national importance from the Swedish Research Council (registration number 2017-00625). JdICR is supported by grants from the Swedish Research Council (2015-03994), the Swedish National Space Board (128/15) and the Swedish Civil Contingencies Agency (MSB). This project has received funding from the European Research Council (ERC) under the European Union's Horizon 2020 research and innovation programme (SUNMAG, grant agreement 759548).

References

- Berghmans, D., van der Linden, R. A. M., Vanlommel, P., et al. 2005, *Annales Geophysicae*, 23, 3115
- Bose, S., Joshi, J., Henriques, V. M. J., & Roupe van der Voort, L. 2021, *A&A*, 647, A147, <http://arxiv.org/abs/2101.07829>
- Brault, J. W. & Neckel, H. 1987, *Spectral Atlas of Solar Absolute Diskaveraged and Disk-Center Intensity from 3290 to 12510 Å*, <ftp://ftp.hs.uni-hamburg.de/pub/outgoing/FTS-Atlas/>
- Bray, T. 2014, *The JavaScript Object Notation (JSON) Data Interchange Format*, RFC 7159, RFC Editor, <https://www.rfc-editor.org/rfc/rfc7159.txt>
- Buehler, D., Esteban Pozuelo, S., de la Cruz Rodríguez, J., & Scharmer, G. B. 2019, *ApJ*, 876, 47, <http://arxiv.org/abs/1905.01245>
- Calabretta, M. 2021, *WCSLIB 7.6*, Australia Telescope National Facility, CSIRO, <http://www.atnf.csiro.au/people/mcalabre/WCS/wcslib.pdf>
- Calabretta, M. R. & Greisen, E. W. 2002, *A&A*, 395, 1077, (WCS Paper II)
- Calabretta, M. R., Valdes, F. G., Greisen, E. W., & Allen, S. L. 2004, *Representations of distortions in FITS world coordinate systems*, https://fits.gsfc.nasa.gov/wcs/dcs_20040422.pdf, (draft dated 2004-04-22)
- Collados, M. 2017, in *SOLARNET IV: The Physics of the Sun from the Interior to the Outer Atmosphere*, 1, <http://research.iac.es/congreso/solarnet-4meeting/>
- Couvidat, S., Schou, J., Hoeksema, J. T., et al. 2016, *Sol. Phys.*, 291, 1887
- Criscuoli, S. & Tritschler, A. 2014, *IBIS Data Reduction Notes*, NSO, https://nosp.nso.edu/sites/nosp.nso.edu/files/files/dst-pipeline/ibis_tn_005.pdf
- de la Cruz Rodríguez, J., Kiselman, D., & M., C. 2011, *A&A*, 528, A113, <http://arxiv.org/abs/1101.2671>
- de la Cruz Rodríguez, J., Leenaarts, J., & Asensio Ramos, A. 2016, *ApJ*, 830, L30, <http://arxiv.org/abs/1609.09527>
- de la Cruz Rodríguez, J., Löfdahl, M., Sütterlin, P., Hillberg, T., & Roupe van der Voort, L. 2015, *A&A*, 573, A40, <http://arxiv.org/abs/1406.0202>
- De Pontieu, B., Title, A. M., Lemen, J. R., et al. 2014, *Sol. Phys.*, 289, 2733
- de Wijn, A. G., de la Cruz Rodríguez, J., Scharmer, G. B., Sliepen, G., & Sütterlin, P. 2021, *The Astronomical Journal*, 161, 89, <http://arxiv.org/abs/2102.01231>
- Denker, C., Kuckein, C., Verma, M., et al. 2018, *ApJS*, 236, 5
- Díaz Baso, C. J. 2018, *PhD thesis*, Universidad de La Laguna, <https://dialnet.unirioja.es/servlet/tesis?codigo=235977>
- Esteban Pozuelo, S., de la Cruz Rodríguez, J., Drews, A., et al. 2019, *ApJ*, 870, 88, <http://arxiv.org/abs/1811.07881>
- Fanning, D. W. 2011, *Coyote's Guide to Traditional IDL Graphics* (Coyote Book Publishing)
- Freeland, S. L. & Handy, B. N. 1998, *Sol. Phys.*, 182, 497

- Gonsalves, R. A. 1982, *Opt. Eng.*, 21, 829
- Górski, K. M., Wandelt, B. D., Hivon, E., Hansen, F. K., & Banday, A. J. 2010, *The HEALPix Primer, Jet Propulsion Laboratory*, v. 2.15a, <https://healpix.jpl.nasa.gov/pdf/intro.pdf>
- Greco, V., Sordini, A., Cauzzi, G., Reardon, K., & Cavallini, F. 2019, *A&A*, 626, A43
- Greisen, E. W. & Calabretta, M. R. 2002, *A&A*, 395, 1061, (WCS Paper I)
- Greisen, E. W., Calabretta, M. R., Valdes, F. G., & Allen, S. L. 2006, *A&A*, 446, 747, (WCS Paper III)
- Hack, W., Dencheva, N., Fruchter, A., & Greenfield, P. 2012, *Distortion Correction in HST FITS Files*, Tech. Rep. TSR 2012-01, Space Telescope Science Institute, https://stwcs.readthedocs.io/en/stable/fits_convention_tsr/source/index.html
- Hartley, R. & Zisserman, A. 2000, *Multiple View Geometry in Computer Vision*, 2nd edn. (Cambridge University Press)
- Haugan, S. V. H. & Fredvik, T. 2015, *Document on Standards for Data Archiving and VO, Deliverable D20.4, SOLARNET (EC 7th FP grant 312495)*
- Haugan, S. V. H. & Fredvik, T. 2020, *ArXiv e-prints [arXiv:2011.12139v1]*
- Heesch, D. S., Howard, W. E., et al. 1973, *Transactions of the IAU*, 15A(2), 165
- Henriques, V. M. J. 2012, *A&A*, 548, A114, <http://arxiv.org/abs/1210.4168>
- Jess, D. & Keys, P. 2017, *ROSA data reduction pipeline*, Queen's University Belfast Astrophysics Research Centre, https://star.pst.qub.ac.uk/wiki/doku.php/public/research_areas/solar_physics/rosa_reduction_pipeline
- Joshi, J., Rouppe van der Voort, L. H. M., & de la Cruz Rodríguez, J. 2020, *A&A*, 641, L5, <http://arxiv.org/abs/2006.14975>
- Kasten, F. & Young, A. T. 1989, *Appl. Opt.*, 28, 4735
- Kianfar, S., Leenaarts, J., Danilovic, S., de la Cruz Rodríguez, J., & José Díaz Baso, C. 2020, *A&A*, 637, A1, <http://arxiv.org/abs/2003.11302>
- Kosugi, T., Matsuzaki, K., Sakao, T., et al. 2007, *Sol. Phys.*, 243, 3
- Kučera, A., Ambróz, J., Gömöry, P., Kozák, M., & Rybák, J. 2010, *Contrib. Astron. Obs. Skalnaté Pleso*, 40, 135, <https://www.ta3.sk/caosp/Eedition/FullTexts/vol40no3/pp135-138.pdf>
- Kučera, A., Tomczyk, S., Rybák, J., et al. 2015, in *IAU General Assembly*, Vol. 29, 2246687
- Kuckein, C., Denker, C., Verma, M., et al. 2017, in *Fine Structure and Dynamics of the Solar Atmosphere*, ed. S. Vargas Domínguez, A. G. Kosovichev, L. Harra, & P. Antolin, *Proc. IAUS No. 327*, <https://arxiv.org/abs/1701.01670>
- Kuridze, D., Mathioudakis, M., Morgan, H., et al. 2019, *ApJ*, 874, 126, <http://arxiv.org/abs/1902.07514>
- Landsman, W. B. 1993, in *ASP Conf. Ser.*, Vol. 52, *Astronomical Data Analysis Software and Systems II*, ed. R. J. Hanisch, R. J. V. Brissenden, & J. Barnes, 246, see also <http://id1astro.gsfc.nasa.gov>
- Leenaarts, J., de la Cruz Rodríguez, J., Danilovic, S., Scharmer, G., & Carlsson, M. 2018, *A&A*, 612, <http://arxiv.org/abs/1712.00474>
- Löfdahl, M. G. 2002, in *Proc. SPIE*, Vol. 4792, *Image Reconstruction from Incomplete Data II*, ed. P. J. Bones, M. A. Fiddy, & R. P. Millane, 146–155, <http://arxiv.org/abs/physics/0209004>
- Löfdahl, M. G. & Scharmer, G. B. 1994, *A&AS*, 107, 243
- Löhner-Böttcher, J., Schmidt, W., Doerr, H.-P., et al. 2017, *A&A*, 607, A12
- Löhner-Böttcher, J., Schmidt, W., Stief, F., Steinmetz, T., & Holzwarth, R. 2018, *A&A*, 611, A4
- Mampaey, B., Vansintjan, R., & Delouille, V. 2017, in *SOLARNET IV: The Physics of the Sun from the Interior to the Outer Atmosphere*, 91, <http://research.iac.es/congreso/solarnet-4meeting/>
- Markwardt, C. B. 2009, in *ASP Conf. Ser.*, Vol. 411, *Astronomical Data Analysis Software and Systems XVIII*, ed. D. A. Bohlender, D. Durand, & P. Dowler, 251
- Neckel, H. 1999, *Sol. Phys.*, 184, 421
- Neckel, H. 2005, *Sol. Phys.*, 229, 13
- Neckel, H. & Labs, D. 1994, *Sol. Phys.*, 153, 91
- Noll, R. J. 1976, *J. Opt. Soc. Am.*, 66, 207
- Paxman, R. G., Schulz, T. J., & Fienup, J. R. 1992a, *J. Opt. Soc. Am. A*, 9, 1072
- Paxman, R. G., Schulz, T. J., & Fienup, J. R. 1992b, in *Technical Digest Series, Vol. 11, Signal Recovery and Synthesis IV*, Optical Society of America, 5–7
- Paxman, R. G., Seldin, J. H., Löfdahl, M. G., Scharmer, G. B., & Keller, C. U. 1996, *ApJ*, 466, 1087
- Pébay, P., Terriberry, T. B., Kolla, H., & Bennett, J. 2016, *Computational Statistics*, 31, 1305
- Pence, W. D., Chiappetti, L., Page, C. G., Shaw, R. A., & Stobie, E. 2010, *A&A*, 524, A42
- Pietrow, A. G. M., Kiselman, D., de la Cruz Rodríguez, J., et al. 2020, *A&A*, 644, A43, <http://arxiv.org/abs/2006.14486>
- Roddier, N. 1990, *Opt. Eng.*, 29, 1174
- Rots, A. H., Bunclark, P. S., Calabretta, M. R., et al. 2015, *A&A*, 574, A36
- Rouppe van der Voort, L., De Pontieu, B., Scharmer, G. B., et al. 2017, *ApJ*, 851, L6, <http://arxiv.org/abs/1711.04581>
- Rouppe van der Voort, L. H. M., De Pontieu, B., Carlsson, M., et al. 2020, *A&A*, 641, A146, <http://arxiv.org/abs/2005.14175>
- Rouppe van der Voort, L. H. M., Joshi, J., Henriques, V. M. J., & Bose, S. 2021, *A&A*, 648, A54, <http://arxiv.org/abs/2101.11321>
- Sanchez Almeida, J. & Lites, B. W. 1992, *ApJ*, 398, 359
- Scharmer, G. 2017, in *SOLARNET IV: The Physics of the Sun from the Interior to the Outer Atmosphere*, 85
- Scharmer, G. B. 2006, *A&A*, 447, 1111
- Scharmer, G. B., Bjelksjö, K., Korhonen, T. K., Lindberg, B., & Pettersson, B. 2003, in *Proc. SPIE*, Vol. 4853, *Innovative Telescopes and Instrumentation for Solar Astrophysics*, ed. S. Keil & S. Avakyan, 341–350
- Scharmer, G. B., Löfdahl, M. G., Slieden, G., & de la Cruz Rodríguez, J. 2019, *A&A*, 626, A55, <http://arxiv.org/abs/1905.05588>
- Scharmer, G. B., Narayan, G., Hillberg, T., et al. 2008, *ApJ*, 689, L69
- Schnerr, R., de la Cruz Rodríguez, J., & van Noort, M. 2011, *A&A*, 534, A45, <http://arxiv.org/abs/1012.1225>
- Selbing, J. 2005, *Master's thesis*, Stockholm University, <http://arxiv.org/abs/1010.4142>
- Seldin, J. H. & Paxman, R. G. 1994, in *Proc. SPIE*, Vol. 2302, *Image reconstruction and restoration*, ed. T. J. Schultz & D. L. Snyder, 268–280
- Slieden, G. & Sütterlin, P. 2013, in *Synergies Between Ground and Space Based Solar Research, 1st SOLARNET – 3rd EAST/ATST meeting*
- Smith, J. D. 2003, *Ninterpolate function*, <https://tir.astro.utoledo.edu/id1/ninterpolate.pro>, see also “Multidimensional Interpolation” thread from 2003 in [news:comp.lang.idl-pvwave](https://comp.lang.idl-pvwave).
- Socas-Navarro, H., de la Cruz Rodríguez, J., Asensio Ramos, A., Trujillo Bueno, J., & Ruiz Cobo, B. 2015, *A&A*, 577, A7, <http://arxiv.org/abs/1408.6101>
- SPICE Consortium, Anderson, M., Appourchaux, T., et al. 2020, *A&A*, 642, A14
- Szydlarski, M. 2019, in *ALMA2019: Science Results and Cross-Facility Synergies*, 126
- Thompson, W. 2010a, *The SolarSoft WCS Routines: A Tutorial*, Adnet Systems, Inc., NASA Goddard Space Flight Center, https://hesperia.gsfc.nasa.gov/ssw/gen/doc/spice/wcs_tutorial.pdf
- Thompson, W. T. 2006, *A&A*, 449, 791
- Thompson, W. T. 2010b, *A&A*, 515, A59
- van Noort, M., Rouppe van der Voort, L., & Löfdahl, M. G. 2005, *Sol. Phys.*, 228, 191
- van Noort, M. J. & Rouppe van der Voort, L. H. M. 2008, *A&A*, 489, 429
- Vissers, G. & Rouppe van der Voort, L. 2012, *ApJ*, 750, 22, <http://arxiv.org/abs/1202.5453>
- Vissers, G. J. M., de la Cruz Rodríguez, J., Libbrecht, T., et al. 2019, *A&A*, 627, A101, <http://arxiv.org/abs/1905.02035>
- Wilkinson, M. D., Dumontier, M., Aalbersberg, I. J., et al. 2016, *Scientific Data*, 3, 160018

Appendix A: Pipeline code

The non-MOMFBD parts of SSTRED are coded in IDL with some parts implemented as DLMs coded in C/C++ for speed and/or for using existing code.

SSTRED uses IDL objects with the major steps in the processing implemented as class methods. There are separate classes for CRISP and CHROMIS, inheriting common code from a top class whenever possible and practical.

Adding support for another, similar instrument should not be very hard. It is a matter of entering information about detectors, file formats, and filters, identifying common processing steps, and writing a few new class methods that cover the differences. Of course, identifying any particular data imperfections for the new instrument and developing calibrations and corrections for them could be time consuming.

Appendix A.1: Required IDL libraries

The following IDL code/libraries are required:

IDLAstro: We use code from the IDL Astronomy User’s Library (Landsman 1993), mainly for manipulating FITS headers and extensions. This library is available through git from [git://github.com/wlandsman/IDLastro.git](https://github.com/wlandsman/IDLastro.git).

Coyote: We make use of mainly plotting routines from the Coyote library (Fanning 2011). The code is available in a maintained version as a git repository at <https://github.com/idl-coyote/coyote>.

Mpfit: Many steps in SSTRED require non-linear model fitting. For some of them we use the Levenberg–Marquardt algorithm as implemented in the IDL mpfit routines by Markwardt (2009), available for download from <http://www.physics.wisc.edu/~craigm/idl/down/mpfit.tar.gz>. (A C version of mpfit is also incorporated in some of the C/C++ code.)

Appendix A.2: DLMs

Some parts of the pipeline are implemented as DLMs coded in C/C++. There are several reasons for this, primarily because it gives access to lower level C++ functionality, which allows for optimization. There is also the benefit of getting access to high level C++ libraries, such as boost and OpenCV. In particular, the pinhole calibration mentioned in 4.1 utilizes *camera calibration tools* readily available in OpenCV.

The DLM also allows direct access to code intrinsic to the REDUX/MOMFBD software. This means we can be certain that function calls within IDL are doing the exact same thing as the redux code does.

Sample tasks implemented as DLMs:

- Sum images.
- Read and mosaic MOMFBD output.
- Read and write fz format files.
- Do pinhole alignment.
- Geometric transform of images.
- Measurements and application of stretch vectors.
- Log file conversion
- Some metadata handling
- Access to some internal redux MOMFBD code.

Appendix A.3: Redux code

CHROMIS and CRISP data are restored from optical aberrations caused by turbulence in the atmosphere and partially corrected by the SST AO.

We have used the MOMFBD code of van Noort et al. (2005) as the workhorse for SST image data for several years. One of us (TH) now maintains a fork of that project (called *redux*), where parts of the original code are replaced with open-source libraries.

Redux implements several improvements and new features compared to MOMFBD. Among them is a method for making sparser null-space matrices from the LECs, leading to a speedup with ~33%. Another is the re-implementation of the extra WB objects used for dewarping (see Sect. 5.4) with an additional ~25% speedup.

As with the old MOMFBD code, pinhole calibration is used to specify the relative geometry between the cameras involved in a data set to be restored. The redux code can read the new projective transforms described in 4.1. (It still supports the xoffs/yoffs files of the old MOMFBD program.)

See <https://dubshen.astro.su.se/wiki/index.php/Redux> for installation and usage instructions.

Appendix B: Wavelength distortions

This appendix describes how SSTRED stores cavity errors (see Sect. 4.2) as distortions in the wavelength coordinate.

The etalons are fixed with respect to the detectors, so the cavity errors can be described as distortions that are a function of the spatial pixel coordinates. But the distorted coordinate is not a pixel coordinate, it is the wavelength in physical units, i.e., the wavelength world coordinate.

Calabretta et al. (2004) defined a notation for describing coordinate distortions as part of the WCS.¹⁹ However, while this notation can specify distortions that are a function of pixel coordinates, the coordinate being distorted also has to be a pixel coordinate.

This would not be a problem if the wavelength pixel-coordinate grid were equidistant in wavelength. Then a distortion in the tuning pixel coordinate would be equivalent to a distortion in the wavelength world coordinate. But in our case, the wavelength is tabulated with no restriction on the spacing between tuning points. This would lead to table look-up that has a discontinuous derivative, defined by the spacing in wavelength between the two nearest tuning points. Alternatively, if the distortion was defined in the tuning pixel coordinate, it would have to be specified for each tuning, resulting in an extra dimension in the distortion table – and that would still cause problems at tuning points surrounded by different-length wavelength intervals.

We use an extended notation, described by (Haugan & Fredvik 2020, version 1.5, in prep.). This notation allows distortions to be *associated* with and *applied* to any of a set of numbered *stages* in the conversion of pixel coordinates to world coordinates in the WCS. In contrast to the cases considered by Calabretta et al. (2004), the associate and apply stages are specified individually. Below we give a brief description focused on the parts used for the cavity errors.

The new notation generalizes the *record-valued* DP_j/DQ_i keywords and the associated CPDIS_j/CQDIS_i keywords of Calabretta et al. (2004) and defines keywords with similar meaning, but with W substituted for P and Q. The DW_j (and *i*) keywords have a few extra records compared to DQ_i and DP_j, namely

¹⁹ Unlike the other WCS papers we refer to, Calabretta et al. (2004) is published only in draft form. However, the notation is in fact used for data from the Hubble Space Telescope (Hack et al. 2012) and will be used for SPICE. It is also implemented in the WCSLIB C library (Calabretta 2021), see <https://www.atnf.csiro.au/people/Mark.Calabretta/WCS/index.html>.

DW*j*-ASSOCIATE and DW*j*-APPLY, the values of which are the relevant stage numbers. See Fig. B.1 for the corresponding part of a FITS header.

The cavity maps are a function of the spatial pixel coordinates at stage 1 (the associate stage) but they are a distortion of the spectral world coordinate at stage 6 (the applied stage). Consequently, we set DW3-ASSOCIATE to 1 and DW3-APPLY to 6.

Following Calabretta et al. (2004), we store the distortion array in a FITS image extension named WCSDVARR. Multiple distortions, to be applied in sequence, can be stored in multiple WCSDVARR extensions with different version numbers (EXTVER keyword). Each distortion array can be defined to apply to only a partial range of the apply coordinates. For this, the DW*j*-SCALE*i* and DW*j*-OFFSET*i* keywords are used (see Calabretta et al. 2004; Haugan & Fredvik 2020 for details). We use this mechanism for the multiple cavity maps resulting from CHROMIS line scans using multiple prefilers (Sect. 4.2.1).

SSTRED has code for reading at least the distortions written by SSTRED itself. It should not be hard to port this to any language in which one wants to read SSTRED output. Documentation can be found in the SST wiki at <https://dubshen.astro.su.se/wiki/index.php/SSTRED>.

The corrected wavelength coordinate for a data pixel, $\lambda_{\text{corr}}(i_x, i_y, i_{\text{tun}}, i_{\text{pol}}, i_{\text{scan}}) = \lambda(i_{\text{tun}}) + \delta\lambda(i_x, i_y, i_{\text{tun}})$, where $\lambda(i_{\text{tun}})$ is the nominal tuning wavelength and $\delta\lambda$ is the contents of the image extension WCSDVARR.

Appendix C: CRISPEX supported file formats

Appendix C.1: Metadata

The CRISPEX program needs metadata for correctly handling and displaying the data. It in particular needs coordinates: spatial, temporal, spectral, and polarimetric.

As the legacy LP format cubes come with a minimalistic header (describing only the cube dimensions and the data type) the CRISPEX IDL command takes a number of keywords, some are boolean flags (to get particular behaviour) and some are used to supply auxiliary data files with additional information (e.g., time in seconds, wavelength values, etc.).

For FITS cubes – both of the IRIS and the SOLARNET compliant varieties – CRISPEX (un)sets such switches and populate auxiliary information variables automatically from the file metadata, thereby simplifying the call sequence. Table C.1 lists which header keywords are used (and how) by CRISPEX. Details are given in Sects. C.1.1 and C.1.2 below.

Appendix C.1.1: IRIS FITS files

Most header keywords are used to determine or read the spatial WCS information that can then be processed by the SolarSoft IDL functions `wcs_get_coord()` and `wcs_get_pixel()` to go back-and-forth between cube pixel and data value, especially for the coordinate transform between files of differently sized FOV. Most other header keywords are used to get correct labelling in plot windows and control panel selection options, or as switches to enable/disable certain behaviour. The remainder are to deal with multiple spectral windows for the particular case of IRIS Level 3 data, where the wavelength axis is usually a concatenation of non-contiguous spectral diagnostic windows corresponding to the various lines observed.

IRIS Level 3 files contain four extensions, the first three of which are used by CRISPEX: (0) the main data (in BUNIT), (1) the wavelength array (in CUNIT3), and (2) the timing array (in

CUNIT4 since STARTOBS). IRIS Level 2 SJI files contain three extensions of which CRISPEX only uses the first two. The main extension again contains the main data. The first auxiliary extension holds the time- and raster step-dependent information on the slit.

Appendix C.1.2: SOLARNET compliant FITS files

The SOLARNET compliant FITS cubes use WCS for all coordinates, see Sect. 6.3. The WCS information is in main header keywords and/or binary extensions, depending on whether it is on regular grids or has to be tabulated.

CRISPEX does not access the WCS headers and extensions directly, but rather retrieves the coordinate information through the SolarSoft functions `fitshead2wcs()` and `wcs_get_coord()`. CRISPEX ensures loading a modified version of `wcs_proj_tab` as well as auxiliary routines (all provided with the CRISPEX distribution) that allow interpolation in the 5-dimensional coordinate look-up table when accessed through `wcs_get_coord()`.

Appendix C.2: Data cube ordering

Irrespective of the file format (LP, IRIS-style FITS, or SOLARNET FITS), CRISPEX expects a certain data cube ordering for it to correctly access the data when moving the cursor or changing, for example, the frame number or wavelength tuning position.

CRISPEX cubes can be written as 3-, 4- or 5-dimensional cubes, but are upon access considered to be 3-dimensional, a sequence of 2-dimensional frames with with any higher dimension combined or “folded” into a third dimension.

At this time, the ordering in the image cubes and spectral cubes is hard-coded. Should the need arise, CRISPEX could be updated to get the ordering information from WCS CTYPE*n* header keywords.

Appendix C.2.1: Image cubes

From the point of view of CRISPEX, the basic data cube is a sequence of 2-dimensional images. With notation from Sect. 3.3, its dimensions are $[N_x, N_y, N_3]$, where $N_3 = N_{\text{tun}} \cdot N_{\text{pol}} \cdot N_{\text{scan}}$. CRISPEX will then subscript the third dimension with index $i_3 = i_{\text{scan}} \cdot N_{\text{tun}} \cdot N_{\text{pol}} + i_{\text{pol}} \cdot N_{\text{tun}} + i_{\text{tun}}$ to get the xy -image at spectrotemporal position $(i_{\text{tun}}, i_{\text{pol}}, i_{\text{scan}})$.

In words, intensity images are stacked according to wavelength tuning first, Stokes parameter second and scan number (i.e., repetition) third. See Fig. C.1 for an illustration involving polarimetric data.

Appendix C.2.2: Spectral cubes

For single-wavelength time-series or single wavelength-scans all dimensions present can be accessed quickly enough that an image cube on its own suffices. However, for multi-dimensional cubes (e.g., time-series of wavelength-scans, or time-series of imaging spectropolarimetry), traversing the image cube to extract the local spectrum or construct the spectrum as function of time for any pixel during run-time would take a considerable amount of time and the recommended procedure is therefore to create a reordered, so-called “spectral”, data cube file for swifter access to the time-dependent spectra.

A CRISPEX spectral cube has dimensions $[N_{\text{tun}}, N_{\text{scan}}, N_3]$, where $N_3 = N_x \cdot N_y \cdot N_{\text{pol}}$. The spectrum-time data frame at


```

CWERR3 = 0.0105497 / [nm] Max total distortion
CWDIS3 = 'Lookup' / WAVE distortions in lookup table

DW3 = 'EXTVER: 1' / Cavity error for 3934
DW3 = 'NAXES: 5' / 3 axes in the lookup table
DW3 = 'AXIS1: 1' / Spatial X
DW3 = 'AXIS2: 2' / Spatial Y
DW3 = 'AXIS3: 3' / Tuning
DW3 = 'AXIS4: 4' / Stokes
DW3 = 'AXIS5: 5' / Scan number
DW3 = 'OFFSET3: 11.0421' / Tuning coordinates offset
DW3 = 'SCALE3: 0.0475238' / Tuning coordinates scale
DW3 = 'CWERR: 0.0139631' / [nm] Max distortion (this correction step)
DW3 = 'CWDIS.LOOKUP: 1' / Distortions in lookup table
DW3 = 'ASSOCIATE: 1' / Association stage (pixel coordinates)
DW3 = 'APPLY: 6' / Application stage (world coordinates)

DW3 = 'EXTVER: 2' / Cavity error for 3969
DW3 = 'NAXES: 5' / 3 axes in the lookup table
DW3 = 'AXIS1: 1' / Spatial X
DW3 = 'AXIS2: 2' / Spatial Y
DW3 = 'AXIS3: 3' / Tuning
DW3 = 'AXIS4: 4' / Stokes
DW3 = 'AXIS5: 5' / Scan number
DW3 = 'OFFSET3: -9.95792' / Tuning coordinates offset
DW3 = 'SCALE3: 0.0475238' / Tuning coordinates scale
DW3 = 'CWERR: 0.0105497' / [nm] Max distortion (this correction step)
DW3 = 'CWDIS.LOOKUP: 1' / Distortions in lookup table
DW3 = 'ASSOCIATE: 1' / Association stage (pixel coordinates)
DW3 = 'APPLY: 6' / Application stage (world coordinates)

```

Fig. B.1: WCS distortions part of a sample FITS header with cavity maps for two Ca II prefilers, 3934 and 3969. These lines go after the CDELTA3 line in Fig. 15.

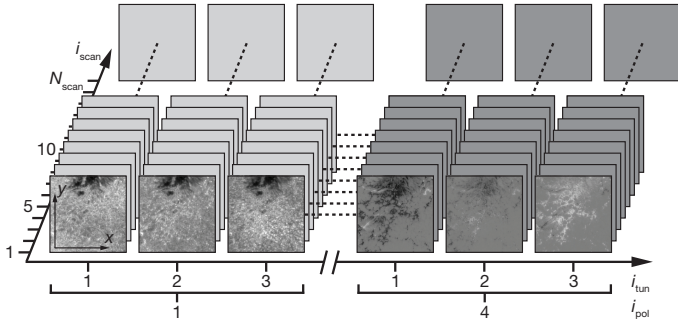


Fig. C.1: Schematic representation of the CRISPEX data ordering of a spectrotemporal Stokes cube with 3 tuning positions. The third dimension has been “unfolded” into a tuning/polarimetry axis and a scan axis, showing that the data are ordered sequentially as wavelength scans for each Stokes parameter separately, before going to the next scan. On the polarimetry axis, $i_{\text{pol}} = [1, 2, 3, 4] \Leftrightarrow$ Stokes $[I, Q, U, V]$ (Q and U not shown in the figure).

position $(i_x, i_y, i_{\text{pol}})$ is obtained by indexing the third dimension with $i_3 = i_y \cdot N_x \cdot N_{\text{pol}} + i_x \cdot N_{\text{pol}} + i_{\text{pol}}$, i.e., spectrum-time diagrams are stacked according to Stokes parameter first, followed by the two spatial dimensions. x -coordinate second and y -coordinate third.

Appendix D: Calculation of mean and moments

In this appendix we detail how we calculate the mean, variance (and its positive square root, the standard deviation from the mean), skewness, and excess kurtosis²⁰ for the SOLARNET statistical keywords. We want to do this for a data cube or a subset

thereof, without having the entire cube in memory at the same time, by combining the same statistics calculated for the individual frames.

This would also potentially be useful for an SVO that supports serving subsets of data defined on the fly.

Following Pébay et al. (2016) we write the mean of a set of n data points as

$$\bar{x} = \sum_{i=1}^n x_i. \quad (\text{D.1})$$

and define the central moments for any $p \geq 2$ as

$$\mu_p = M_p/n, \quad (\text{D.2})$$

where

$$M_p = \sum_{i=1}^n (x_i - \bar{x})^p. \quad (\text{D.3})$$

We partition the n data points into two subsets \mathcal{A} and \mathcal{B} with $n_{\mathcal{A}}$ and $n_{\mathcal{B}}$ data points, respectively, and define $\bar{x}_{\mathcal{A}}$ ($\bar{x}_{\mathcal{B}}$) and $M_p^{\mathcal{A}}$ ($M_p^{\mathcal{B}}$) are as \bar{x} and M_p , but for the subset \mathcal{A} (\mathcal{B}). We also define

$$\delta_{\mathcal{B},\mathcal{A}} = \bar{x}_{\mathcal{B}} - \bar{x}_{\mathcal{A}}. \quad (\text{D.4})$$

²⁰ The kurtosis for a normal distribution is 3. It is common to subtract 3 to get 0 for the normal distribution. The result is referred to as the *excess kurtosis* and this is the quantity returned by the IDL `kurtosis()` and `moment()` functions, as well as by default by python’s `scipy.stats.kurtosis()` function. See www.harrisgeospatial.com/docs/moment.html and docs.scipy.org/doc/scipy/reference/generated/scipy.stats.kurtosis.html.

Table C.1: FITS header keywords required by CRISPEX

Keyword	SN	SG	SJ	Description and use
BITPIX	X	X	X	Number of bits per pixel; is converted to IDL datatype and used to initialise variables holding the data slices
NAXIS <i>i</i>	X	X	X	Numbered variables specifying the size of each dimension
BTYPE	X	X	X	Description of data type, e.g., intensity, temperature, pressure, etc.; used for plot labelling and user feedback
BUNIT	X	X	X	Data units, e.g., erg cm ⁻² s ⁻¹ sr ⁻¹ , K, m s ⁻¹ , etc.; used for plot labelling and user feedback
BSCALE	X	—	X	Data scaling factor; used in combination with BZERO to descale the data
BZERO	X	—	X	Data scaling offset; used in combination with BSCALE to descale the data
CDEL <i>Ti</i>	X	X	X	Pixel size of each dimension in terms of CUNIT <i>i</i> ; used for WCS transformations (pixel-to-WCS and vice versa)
CRPIX <i>i</i>	X	X	X	Reference pixel of each dimension; used for WCS transformations
CRVAL <i>i</i>	X	X	X	Reference pixel value of each dimension in terms of CUNIT <i>i</i> ; used for WCS transformations
CTYPE <i>i</i>	X	X	X	Description of data type of each dimension; used for plot labelling and user feedback (the CTYPE <i>i</i> corresponding to the X-axis is also checked for containing 'TAB', to determine further processing)
CUNIT <i>i</i>	X	X	X	Data unit of each dimension (e.g., arcsec, Ångström, seconds, etc.); used for plot labelling and user feedback
PC <i>i_j</i>	X	X	X	Elements of the PC-matrix; used in WCS transformations
OBSID	—	X	X	IRIS observing program ID; provided in user feedback
STARTOBS	P	X	X	Date and time of observations start; used to determine the timing in UTC when combined with second (first) auxiliary extension data of a SG (SJI) file.
DATE_OBS	X	X	X	Date and time of observations start; used if STARTOBS is not defined
INSTRUME	X	X	P	Instrument that produced the data; used to (un)set the non-equidistant spectral warping switch for IRIS SG data (unset if not equal to 'IRIS')
NWIN	—	X	—	Number of diagnostics compressed in the wavelength dimension
WSTART <i>i</i>	—	X	—	Starting index of each diagnostic; used in combination with WWIDTH <i>i</i> to determine diagnostic boundaries within the spectral dimension
WWIDTH <i>i</i>	—	X	—	Width in pixels of each diagnostic; used in combination with WSTART <i>i</i> to determine diagnostic boundaries within the spectral dimension
WDESC <i>i</i>	—	X	—	Label of each diagnostic; used in labelling plots and control panel selection options
TWAVE <i>i</i>	—	X	—	Central wavelength of each diagnostic; used to determine the Doppler velocity
TDESC1	—	—	X	Label of detector; used for control panel labelling of SJI functions
TELESCOP	P	—	X	Telescope name; used for control panel labelling of SJI functions
TIME	—	—	X	Time since STARTOBS, keyword indicates the row-index of the extension data array; used to determine the timing in UTC
XCENIX	—	—	X	Time-dependent central FOV X-value in CUNIT1 (row-index); used to determine the SJI CRVAL1
YCENIX	—	—	X	Time-dependent central FOV Y-value in CUNIT2 (row-index); used to determine the SJI CRVAL2
PC <i>i_j</i> IX	—	—	X	Time-dependent PC-matrix elements (row-index); used determine the SJI CRPIX/2, and by extension CRVAL1/2
SLTPX1IX	—	—	X	Time-dependent slit center X-pixel (row-index); used to determine the SJI CRPIX1 and CRVAL1
SLTPX2IX	—	—	X	Time-dependent slit center Y-pixel (row-index); used to determine the SJI CRPIX2 and CRVAL2

Notes. Columns 2–4 indicate whether a particular keyword is required (marked X), present but not required / actively used (marked P), or absent (marked —) for the SOLARNET (SN), IRIS spectrograph (SG) and slit-jaw image (SJ) files, respectively. The keywords above the horizontal line are from the main data extension header; those below that correspond to the first auxiliary extension header. For tabulated WCS coordinates, the keywords CDEL*Ti*, CRPIX*i*, and CRVAL*i* are defined differently, along with PS*i_j* and PV*i_j* they are used to find the relevant data in binary extensions (see Greisen et al. 2006).

With those definitions, Pébay et al. (2016) write “pairwise and update formulas” for the mean value of the n data points as the following combination of the means for the two subsets,

$$\bar{x} = \bar{x}_{\mathcal{A}} + \frac{n_{\mathcal{B}}}{n} \delta_{\mathcal{B},\mathcal{A}}, \quad (\text{D.5})$$

and n times the central moments as

$$M_p = M_p^{\mathcal{A}} + M_p^{\mathcal{B}} + n_{\mathcal{A}} \left(\frac{-n_{\mathcal{B}}}{n} \delta_{\mathcal{B},\mathcal{A}} \right)^p + n_{\mathcal{B}} \left(\frac{n_{\mathcal{A}}}{n} \delta_{\mathcal{B},\mathcal{A}} \right)^p + \sum_{k=1}^{p-2} \binom{p}{k} \delta_{\mathcal{B},\mathcal{A}}^k \left[M_{p-k}^{\mathcal{A}} \left(\frac{-n_{\mathcal{B}}}{n} \right)^k + M_{p-k}^{\mathcal{B}} \left(\frac{n_{\mathcal{A}}}{n} \right)^k \right]. \quad (\text{D.6})$$

We use equations (D.5) and (D.6) repeatedly, to incrementally calculate the statistics for the whole cube one frame at a time. The mean, \bar{x} , as defined above for a data cube with n pixels is what we need. But the variance, skewness, and excess kurtosis

are not the same as the central moments, μ_p , although the conversions are easy enough. By definition, the unbiased estimate of the variance can be written as

$$\sigma^2 = \frac{1}{n-1} \sum_i (x_i - \bar{x}_m)^2 \equiv \mu_2 \frac{n}{n-1} \quad (\text{D.7})$$

and the standard deviation is its positive square root, σ . The Fisher–Pearson coefficient of skewness is defined as

$$s = \frac{1}{n} \sum_i \left(\frac{x_i - \bar{x}}{\sigma} \right)^3 \equiv \mu_3 \sigma^{-3}. \quad (\text{D.8})$$

and the excess kurtosis as

$$k = \frac{1}{n} \sum_i \left(\frac{x_i - \bar{x}}{\sigma} \right)^4 - 3 \equiv \mu_4 \sigma^{-4} - 3. \quad (\text{D.9})$$